Ore Geology Reviews 143 (2022) 104750

Contents lists available at ScienceDirect

Ore Geology Reviews

journal homepage: www.elsevier.com/locate/oregeorev

Mineral Paragenesis, formation stages and trace elements in sulfides of the Olympiada gold deposit (Yenisei Ridge, Russia)

Sergey A. Silyanov [a,*], Anatoly M. Sazonov [a], Evgeny A. Naumov [b], Boris M. Lobastov [a], Yelena A. Zvyagina [a], Dmitry A. Artemyev [c], Natalia A. Nekrasova [a], Franco Pirajno [d]

[a] Institute of Mining, Geology and Geotechnology, Siberian Federal University, 660041 Krasnoyarsk, Russia
[b] Central Research Institute of Geological Prospecting for Base and Precious Metals, 117545 Moscow, Russia
[c] Institute of Mineralogy South Urals Research Center of Mineralogy and Geoecology of the Urals Branch of the Russian Academy of Sciences, 456317 Miass, Russia
[d] Centre for Exploration Targeting, University of Western Australia, 6009 Perth, Australia

ARTICLE INFO

Keywords:
Yenisei Ridge
Olympiada Gold Deposit
Sulfides
"Invisible" Gold
Trace Elements
LA-ICP-MS

ABSTRACT

The mineral sequence and LA-ICP-MS study of the trace-elements distribution in chalcogenides (arsenopyrite, pyrite, pyrrhotite, sphalerite, chalcopyrite, ullmannite, tetrahedrite, berthierite, stibnite, gudmundite, jamesonite) of the Olympiada gold ore deposit (Yenisei Ridge, Russia) are presented. The deposit was formed in three stages, separated by tectonic breaks. Early (I) corresponds to the paragenesis of acicular arsenopyrite + pyrite + pyrrhotite. At the stage of base-metal sulfides (II), the deposition of the bulk of chalcopyrite, sphalerite and galena occurred. Mineral associations of these stages determined the gold-arsenic (Au-As) type of ores. The stage of late sulfides (III) is characterized by the paragenesis of antimony minerals (stibnite + berthierite + gudmundite) and corresponds to the gold-antimony (Au-Sb) ore type. Commercial concentrations of gold were formed at the early sulfides stage in the lattice bonded and nanosize mode in acicular arsenopyrite (12.5–1,512 ppm). The progress of the ore deposition process with the formation of late polymetallic and stibnite-berthierite mineralization led to recrystallization of early sulfides (prismatic arsenopyrite Au ~ 36.4 ppm → dipyramidal arsenopyrite Au ~ 0.5 ppm), remobilization and re-deposition of gold in a native form. Pyrite of the deposit does not contain significant amounts of gold (~0.4 ppm). Silver is absent in early sulfides, but is concentrated in tetrahedrite (348.0–3,811 ppm), jamesonite (0.1–7.7 ppm), berthierite (0.1–2.3 ppm) and stibnite (0.2–2.0 ppm) of the later stage (III). Early sulfides (stage I) are characterized by the As-Au-W-Se-Te geochemical association; polymetallic sulfides (stage II) — by the Cu-Zn-Pb-Cd-In association; and late sulfides (stage III) — by the Sb-Co-Ni-Te-Bi-Pb-Hg-Ag association.

1. Introduction

The Olympiada gold deposit is located within the Eastern gold-bearing belt of the Yenisei Ridge (Krasnoyarsk Territory, Russia) and it's the largest in the world. As of today, its reserves amount to about 1,000 tonnes of Au, and the ore intersections at depths of over 1,500 m allow forecasting a further increase in reserves (Sazonov et al., 2019b; Sazonov et al., 2020). The deposit has a unique constitution of the ores, a complicated geological structure and a long-term multistage formation process.

The history of studying the Olympiada deposit extends for >50 years (since 1968–1974). During this period many aspects of geology and ore genesis were covered to varying degrees, but in the modern scientific geological literature there is a limited amount of data about the deposit. Recent works (Savichev et al., 2006; Borisenko et al., 2014; Yakubchuk et al., 2014; Naumov et al., 2015; Gibsher et al., 2019a, b; Sazonov et al., 2019b; Sazonov et al., 2020) focus on the geological structure of the deposit, the thermodynamics of mineralization, age limits of ore formation and its sources.

Meanwhile, the mineralogical and geochemical features of the deposit are as yet not fully understood (Silyanov et al., 2021a). The mineralogy of the upper horizons of the deposit was previously characterized by L.V. Li, Yu.I. Novozhilov, A.M. Gavrilov, A.D. Genkin, V.G. Mikheev, E.A. Zvyagina and others (Genkin et al., 1994; Novozhilov & Gavrilov, 1999; Grigorov, 2002; Savichev and Gavrilenko, 2003; Li, 2003; Savichev, 2004; Savichev et al., 2006; Novozhilov et al., 2014 *etc.*)

* Corresponding author.
E-mail address: silyanov-s@mail.ru (S.A. Silyanov).

https://doi.org/10.1016/j.oregeorev.2022.104750
Received 24 January 2021; Received in revised form 27 January 2022; Accepted 1 February 2022
Available online 5 February 2022

Now the deep horizons of the deposit have been explored (up to –400 m). Information about mineralogy of these ores is limited. Therefore, the first task of our work is focused on the study of the mineralogy of gold-sulfide ores of deep horizons of the deposit.

Data on the distribution of trace elements (primarily Au) in sulfide minerals of the deposit are also extremely limited. The Au contents in arsenopyrite, pyrrhotite, and pyrite were determined mainly by INNA, ICP-MS and atomic absorption, with the exception of single analyzes of arsenopyrite and pyrite by SIMS (Genkin et al., 1994; Genkin et al., 1998; Novozhilov & Gavrilov, 1999; Genkin et al., 2002; Silyanov et al., 2021a).

Today, one of the main approaches to the studying gold deposits is to combine mineralogy and geochemistry methods using LA-ICP-MS. The LA-ICP-MS method is one of the most powerful tools for the paragenetic analysis of trace elements, determination of basic carrier minerals and concentrators of Au, its associations and sources. A large number of publications with the results of such works demonstrate the validity and efficiency of such studies (Sung et al., 2009; Large et al., 2011; Gregory et al., 2015; Meffre et al., 2016; Maslennikov et al., 2017; Augustin & Gaboury, 2019; Gregory et al., 2019a; Wu et al., 2019; Large &

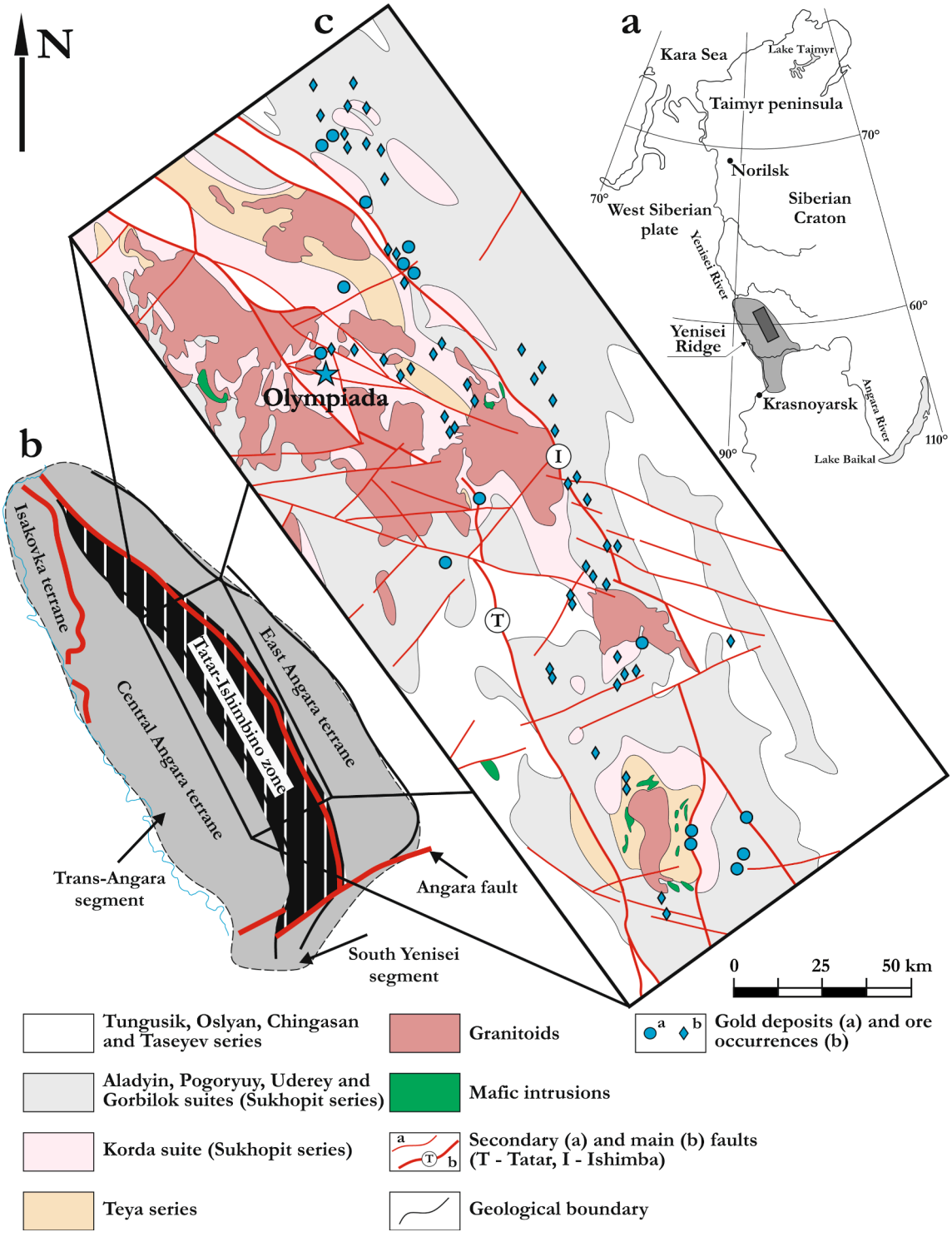

Fig. 1. Yenisei Ridge: a – geographical position; b – tectonic map (Vernikovsky et al., 2016, simplified); c – schematic geologic map of the Eastern gold-bearing belt.

Maslennikov, 2020; Gourcerol et al., 2020 *etc.*).

Thus, large-scale studies of the distribution of gold mineralization and trace-elements in sulfides of various stages of ore formation have not previously been carried out for the Olympiada deposit. On this basis, the second task of our work carried out the first LA-ICP-MS study of the distribution of trace elements in arsenopyrite, pyrite, pyrrhotite, sphalerite, chalcopyrite, ullmannite, tetrahedrite, berthierite, stibnite, gudmundite and jamesonite, collected from the ores of deep horizons in the Eastern part of the Olympiada deposit.

Thus, the main goal of our work is to construct a genetic model of the formation of gold-sulfide parageneses, as well as the development and evolution of the hydrothermal ore system, based on the results of detailed mineralogical and geochemical studies.

2. Geological background

2.1. Geology of the Yenisei Ridge

The Yenisei ridge is a Neoproterozoic (860–800 Ma) collisional orogen that changed to an extensional setting around ~ 750–680 Ma (Metelkin et al., 2007; Likhanov et al., 2014; Kuzmichev & Sklyarov, 2016; Vernikovsky et al., 2016; Nozhkin et al., 2017; Kozlov et al., 2020). The Yenisei Ridge consists of two large segments: South Yenisei and Trans-Angara, which are separated by the ENE striking Angara fault (Fig. 1). The main gold ore bodies are located in the Trans-Angara part as a belt along the eastern edge of the structure (Eastern gold belt of the Yenisei Ridge).

In the tectonic structure of the ridge, the East-Angara, Central-Angara and Isakov terranes are distinguished, the boundaries of which are long-lived deep faults (Ishimba, Tatar, Pri-Yenisey and Ankinovsky) of mainly NW orientation and subvertical dip (Likhanov et al., 2014; Vernikovsky et al., 2016). Gold mineralization is tectonically controlled by the Tatar-Ishimba fault zone, which has a dynamic impact on most of deposits in the region (Sazonov et al., 2020).

The oldest lithologic and stratigraphic subdivisions of the Trans-Angara part of the Yenisei Ridge are Early Cambrian gneisses and slates of the Teya series, which are overlain by thick (15–17 km) Meso- and Neoproterozoic rocks of the Sukhopit, Tunguska, Oslyan, Chingasan and Taseyev series (Nozhkin et al., 2011). The deposits of terrigenous, carbonaceous-terrigenous and carbonate-terrigenous composition of the Kordinsky, Gorbilok and Uderey suites of the Sukhopit series (Early and Middle Ripehan) are the most productive for gold mineralization (Sazonov et al., 2010).

Intrusions of ultramafic to felsic and alkaline composition occur in the region, among which syn- and post-collision granitoids formed in the interval of 880–455 Ma prevail (Vernikovsky et al., 2003; Vernikovsky & Vernikovskaya, 2006; Sazonov et al., 2010). Gold deposits are located at distances from 1.5 to 18.0 km from intrusive granitoid bodies, and their genetic relationship is still under discussion (Konstantinov et al., 1999; Li, 2003; Zabiyaka et al., 2004; Serdyuk et al., 2010; Sazonov et al., 2010; Nozhkin et al., 2011).

2.2. Geology of the Olympiada gold deposit

The Olympiada gold deposit is situated 430 km north from the city of Krasnoyarsk in the taiga-dominated mountainous area in the Yenisei Ridge (Fig. 1). It is part of the Verkhnee Enashimo mineral district in the eastern portion of the Central Angara terrane.

The ore field of the deposit is limited to the NW and SW by large NW faults, which are part of the Tatar deep fault system, and it is squeezed from the SW and NW between the Chirimbinsky and Tyradinsky granite massifs. The structure of the ore field is defined by the conjugation of three folds (Innokentyevsky and Chirimbinsky synclines and Medvezhinsky anticline between them), forming an open W-shaped structure. The limbs of the folds are outlined by NW, NE and broadly W-E faults.

Olenye (Au-W), Vysokoe-2 (W), Innokentievskoe (Au-Sb), Tyradinskoe (Au-Sb) and Titimukhta (Au-Bi) deposits are also located within the ore field.

On the surface, the Olympiada deposit consists of two spatially separated parts, Western and Eastern, which are joined at a depth (Intermediate). The deposit is localized within Medvezhinsky anticline complicated by inter-stratal tectonic zones. The core of the fold is composed of quartz-two-mica slates, and quartz-mica-carbonate slates with strata and lenticular interlayers of marmorized limestones and quartz-mica-carbonate slates developed on the limbs (Fig. 2). Ore bodies of the deposit are confined to the limbs and the hinge part of the fold (Sazonov et al., 2019b; Sazonov et al., 2020).

Eastern Olympiada is the main part of the deposit — constituting about 90% of all gold reserves (ore body No. 4). The site is located in the hinge of the Medvezhinsky anticline complicated by the junction of broadly EW, NE and NW faults. The ore body has a saddle shape with bulges in the hinge part and limbs with uneven length (Fig. 2) on the surface in the horizontal section. At a depth, while maintaining its saddle shape, it steeply plunges southward in the form of a column at an angle of 65–75° (Fig. 3).

Ore bodies are localized in zones of quartz-mica-carbonate metasomatically altered rocks, where the content of disseminated sulfides varies from 2 to 7%. In the underlying quartz-garnet-two-mica slates and overlapping quartz-mica-carbonate slates, mineralization is observed only near their contact with carbonate- bearing and carbonate rocks (Fig. 3). Visually, ore bodies are identified on the basis of the occurrence of abundant sulfide mineralization, mainly arsenopyrite, pyrite, pyrrhotite, and stibnite, but the boundaries of ore bodies are determined by sampling.

In terms of ore properties, the predominance of main ore components and minerals, as well as formation conditions, several types of ores are distinguished in the deposit. Gold-arsenic ores (Au ~ 3.9 g/t; native gold fineness 910 to 1,000‰) correspond to the fields of development (Fig. 3, b) of the early mineral association — fine acicular and prismatic arsenopyrite, pyrrhotite and pyrite with subordinate polymetallic sulfides. Gold-antimony ores (~2.9 g/t; native gold fineness 650 to 760‰) are represented by late aggregates of stibnite and berthierite often forming ore breccias. Increased concentrations of Au (up to ~ 5.4 g/t) are observed in the ore intervals of the combined gold-arsenic-antimony mineralization (Sazonov et al., 2019b; Sazonov et al., 2020).

Gold in primary sulfide ores is mainly fine (~10 μm). Free gold in crushed (minus 0.074 mm) ore makes about 15%, up to 45% is present in the cyanidable form in aggregates with ore minerals, and the amount of refractory non-cyanidable gold reaches 39–60% (Sazonov et al., 2019b; Sazonov et al., 2020).

More detailed information about the deposit geology can be found in (Novozhilov and Gavrilov, 1999; Li, 2003; Savichev et al., 2006; Gibsher et al., 2019a, b; Sazonov et al., 2019b; Sazonov et al., 2020; Silyanov et al., 2021a; b).

2.3. Previous data for mineralogy of the Olympiada gold deposit

Ore minerals occur as fine crystalline-granular disseminations, as well as massive segregations in silicified carbonate rocks. The total sulfide content in ores is about 3–5% (Genkin et al., 1994; Novozhilov & Gavrilov, 1999; Grigorov, 2002; Savichev & Gavrilenko, 2003; Li, 2003; Savichev, 2004; Savichev et al., 2006; Sovmen et al., 2009; Novozhilov et al., 2014).

The main minerals in the deposit are arsenopyrite and pyrrhotite. Their quantitative ratios differ based on where in the deposit they are and how close to mineralization. It is noted that pyrrhotite predominates in low-grade ores. Stibnite and berthierite are subordinate and are confined to the upper horizons of ore bodies. Small amounts of sphalerite, chalcopyrite, galena, goodmundite, tetrahedrite, native antimony, pentlandite, violarite, breithauptite, bournonite, cubanite, molybdenite, jamesonite, and other minerals are noted (Genkin et al., 1994; Novozhilov & Gavrilov, 1999; Grigorov, 2002; Savichev & Gavrilenko, 2003;

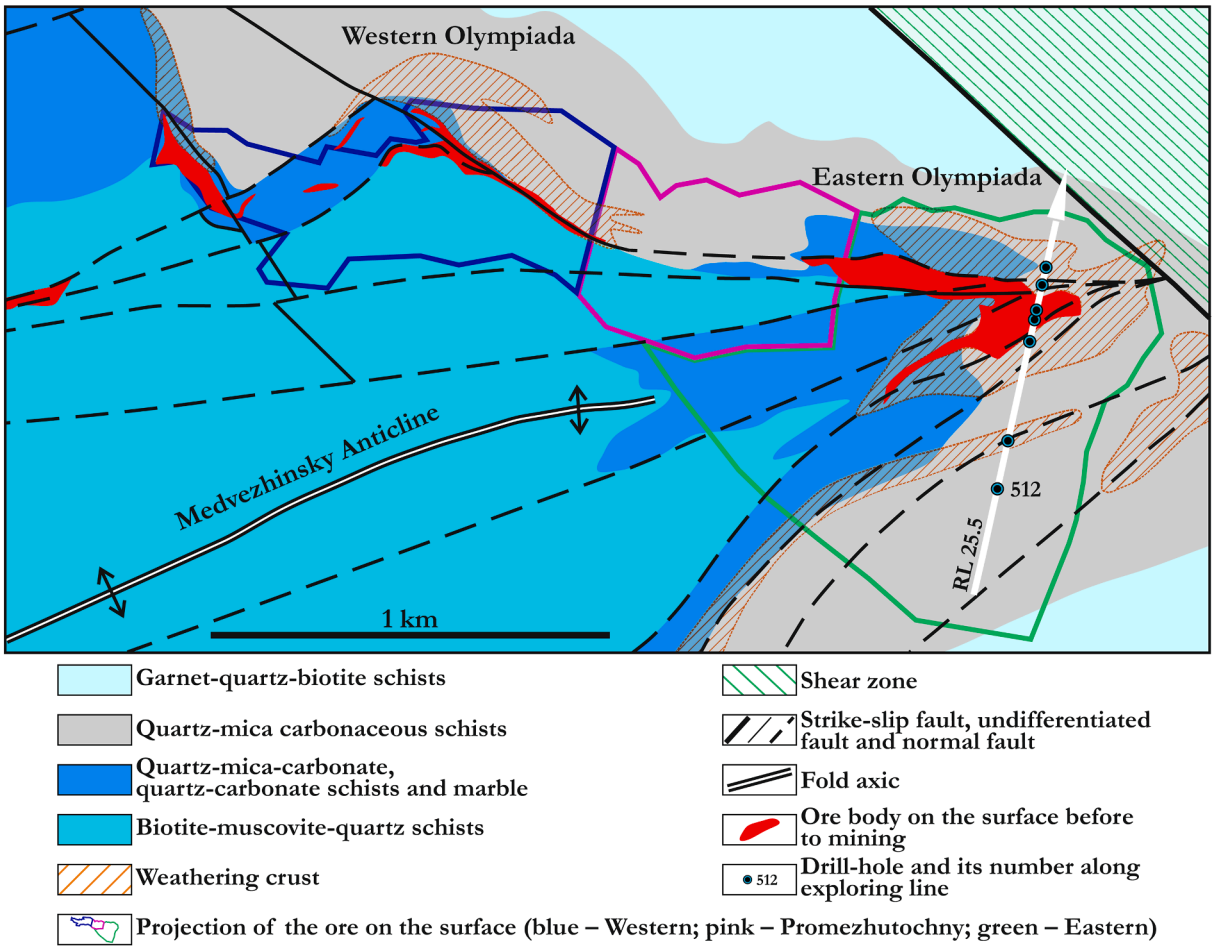

Fig. 2. Geological map of the Olympiada gold deposit (Sazonov et al., 2020). See Fig. 3 for the cross sections along line RL 25.5.

Li, 2003; Savichev, 2004; Savichev et al., 2006; Novozhilov et al., 2014). All of these works indicate the presence of two types of ores – early Au-As and late Au-Sb.

Early work performed on the material of the upper horizons of the Olympiada, as well as at the Olenye (Au-W), Vysokoe-2 (W) and Innokentievskoe (Au-Sb) deposits, show the presence of abundant tungsten mineralization up to ore grade in some areas.

There are several sequences of mineralization within the ore field of the deposit. Savichev (Savichev & Gavrilenko, 2003; Savichev, 2004; Savichev et al., 2006) identified six stages of ore formation: I pre-ore metasomatic changes; II early ore (wolframite-quartz); III main ore (gold-scheelite-sulfide); IV minor ore (gold-sulfosalt-quartz); V late ore (gold-stibnite-quartz); VI post-ore. Novozhilov and Gavrilov (Novozhilov & Gavrilov, 1999; Grigorov, 2002) proposed six paragenetic associations: I pre-ore (sphalerite-chalcopyrite-pyrrhotite); II early pre-productive non-gold bearing (pyrite-arsenopyrite); III early pre-ore (arsenopyrite with "invisible" gold); IV interproductive pyrite; V late productive gold-stibnite; VI post-ore fluorite-carbonate. Baranova et al. (Baranova et al., 1997) identified the following stages: I pre-ore (quartz, calcite, muscovite); II early ore (scheelite, pyrrhotite, arsenopyrite, gold, chalcopyrite, sphalerite, stibnite); III late ore (berthierite, gold, antimony, aurostibite, gudmundite, scheelite); IV post-ore (quartz, calcite, fluorite). The works of Sovmen et al. (Sovmen et al., 2009) identified at the deposit an early gold-sulfide (mainly pyrrhotite-arsenopyrite) association and a late, sulfoantimonide-polymetallic association associated with stibnite, berthierite, ulmannite, goodmundite, tellurides, and base-metal sulfides. In our opinion, the main disadvantage of the above schemes is their generalization to all deposits of the ore field. In this paper, we propose an alternative sequence of mineralization based on the study of ores from deep horizons of the Olympiada deposit.

We do not consider here the mineralogy of oxidized ores, which was described in our previous work (Silyanov et al., 2021b).

3. Samples and analytical methods

3.1. Sampling approach

The mineralogy and stages of ore formation are characterized on the basis of the results of mineralogical study of about 500 polished sections made from the core of twelve exploration drill from the deep horizons of the deposit (Figs. 2 & 3). Optical studies were performed on Carl Zeiss Axioskop 40A Pol and Olympus BX53 microscopes at the Siberian Federal University, Krasnoyarsk.

Samples for our study were taken from the core of exploratory drill 503, which crosses the main ore body of the Eastern (Vostochny) Olympiada in its full thickness (Figs. 2 & 3). In total, 63 polished samples were made from the depth interval of 1.5 to 509.2 m (drillhole depth 538.0 m), including the main sulfide minerals of the deposit at all stages of ore formation (see Section 4.1). Epoxy blocks containing polished fragments were initially viewed under an optical microscope in order to select specific grains for analysis as well as to clarify the paragenetic association and position in the mineral formation stages. The selected grains were then studied using SEM EDS and LA-ICP-MS.

In each sample, from one to ten-point LA-ICP-MS analyses were performed. Depending on the common mineral associations, from one to three coexisting minerals were analyzed in the sample.

The distribution of trace elements was studied in the main ore minerals of the deposit, namely: arsenopyrite, pyrite, pyrrhotite,

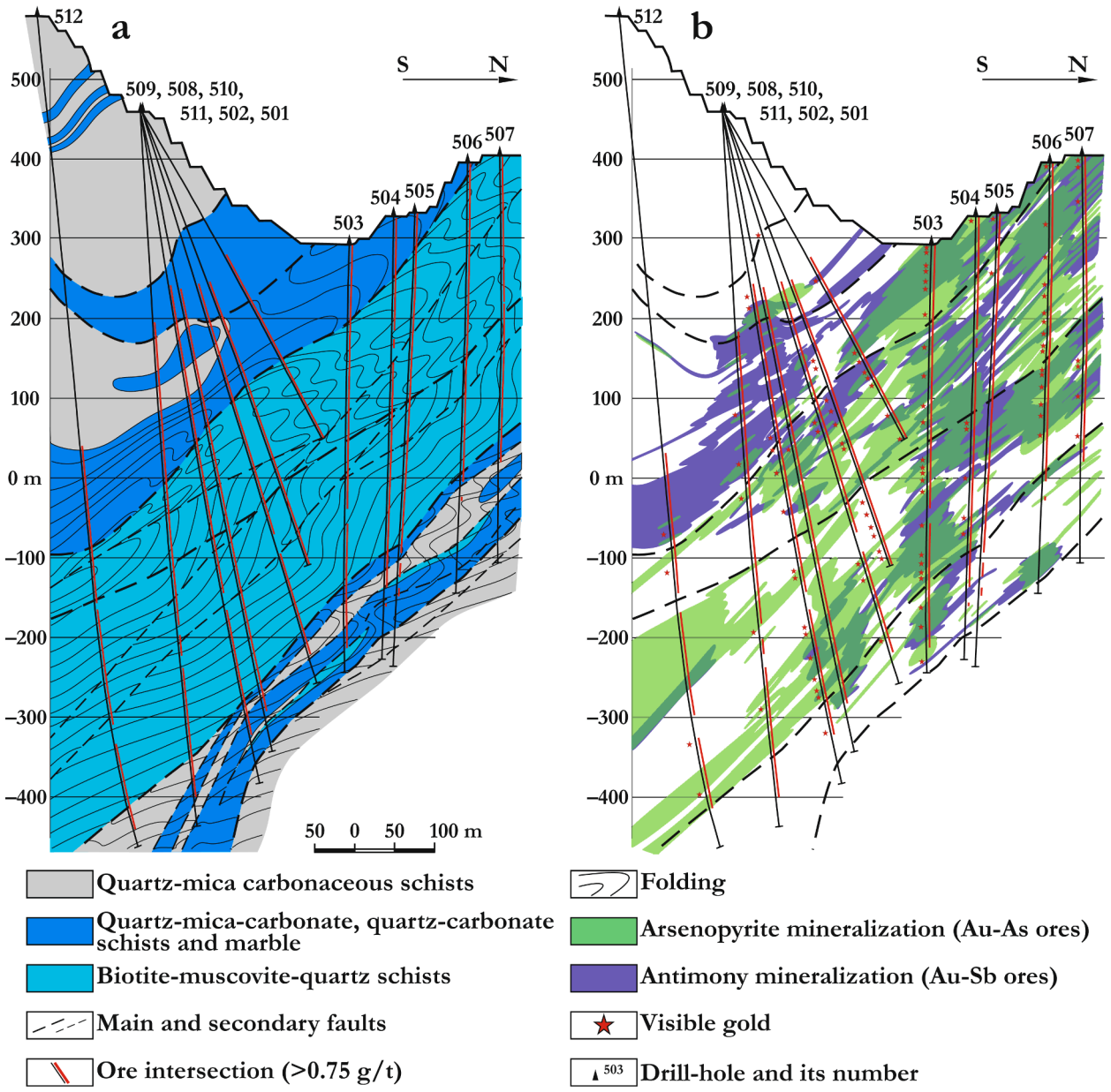

Fig. 3. Cross sections of the Eastern Olympiada, along line RL 25.5 in Fig. 2: a — structural-lithologic pattern (Sazonov et al., 2020); b — ore mineral associations distribution scheme.

sphalerite, chalcopyrite, ullmannite, tetrahedrite, berthierite, stibnite, gudmundite, and jamesonite.

3.2. SEM EDS

The major element compositions of individual sulfide grains were analyzed using SEM (Tescan Vega III SBH with EDS Oxford X-Act) in the R&D Nornickel SibFU Krasnoyarsk, Russia (analysts S.A. Silyanov). The analytical conditions were the following: accelerating voltage of 20 kV, beam current of 1.2 nA and 120 s measuring time. X-ray lines were used to analyze the different elements of S (Kα), Fe (Kα), Co (Kα), Ni (Kα), Cu (Kα), Zn (Kα), As (Lα), Sb (Lα) and Pb (Mα). Pure elements (Co, Ni), as well as FeS, FeS_2, FeAsS, ZnS, $CuFeS_2$, Sb_2S_3, PbTe were used as internal standards; detection limit was 0.05 wt%. Analysis data were processed using Oxford Instruments software.

3.3. LA-ICP-MS

The trace elements in sulfides were studied using a New Wave Research UP-213 (USA) laser ablation system, coupled with an Agilent 7700x (Agilent Technologies, Santa Clara, CA, USA) plasma mass spectrometer in the Institute of Mineralogy SU FRC MG UB RAS Miass, Russia (analysts D.A. Artemyev). The measurements were carried out with an Nd: YAG UV source, frequency quadrupled (wavelength 213 nm) with fluence settings of 1.8–5.5 J/cm^2 (for pyrite, pyrrhotite, stibnite, ullmannite, jamesonite, gudmundite – 1.8–3.0 J/cm^2; for chalcopyrite, arsenopyrite – 3.0–4.5 J/cm^2; for sphalerite – 4.0–5.5 J/cm^2), helium cell carrier gas and a flow rate of 0.50–0.65 L/min. Mass spectrometer settings were as follows: RF Power – 1,550 W; carrier gas – Ar; flow rate – 0.8–0.9 L/min; plasma gas flow (Ar) – 15 L/min; auxiliary gas flow (Ar) – 0.9 L/min.

Each analysis (spot or line with length from 60 to 1,500 μm and ablation speed 1–10 μm/s) was performed with a laser spot size of 25–110 μm diameter at a frequency of 5–10 Hz. The analysis time for

each sample was 90 s, comprising a 30 s measurement of the background and a 60 s analysis. A pre-ablation of 3–4 s was carried out prior to each analysis; a 70–120 s washout took place between analyses as well as pre-ablation and analyses. Calibration of the mass-spectrometer was performed using calibration multi-element solutions and reference material NIST SRM-612. Production of molecular oxide species (i.e., $^{232}Th^{16}O/^{232}Th$) and doubly-charged ion species (i.e., $^{140}Ce^{++}/^{140}Ce^{+}$) was maintained at levels below 0.2%. The $^{238}U/^{232}Th$ ratio with NIST SRM-612 adjustment was 1:1. The external calibration standard USGS MASS-1 (Wilson et al., 2002) and NIST SRM-610 was analyzed every 10–15 spots to account for the instrument drift. All mass fractions for NIST SRM-612, NIST SRM-610 and USGS MASS-1 were taken from the GeoReM base preferred values.

Different spot sizes were used for different minerals, depending on the grain size of that mineral. Large ablation spot sizes of 80–110 μm (pyrite, arsenopyrite, gudmundite) were used for greater composition averaging, in particular for pyrite and arsenopyrite, which can be zoned. For some minerals, "Line mode" was also used to allow for possible zoning. For the rest of the minerals, predominantly the size of the craters was 55–60 μm (pyrite, pyrrhotite, chalcopyrite, sphalerite, arsenopyrite, ullmannite, jamesonite, berthierite, stibnite), and only a few particularly small grains were investigated with a size of 25–30 μm (pyrrhotite). Average LOD are presented in Table A.1.

Arsenopyrite were measured last after pyrite, pyrrhotite, chalcopyrite, sphalerite. Antimony-containing minerals also were measured after low-antimony minerals.

Data processing was carried out using the Iolite software package (Paton et al., 2011). As an internal reference use: ^{57}Fe for pyrite, pyrrhotite, chalcopyrite, arsenopyrite, gudmundite; ^{66}Zn for sphalerite; ^{65}Cu for tetrahedrite; ^{208}Pb for jamesonite; ^{60}Ni for ullmannite; ^{34}S for stibnite. ^{34}S used as an internal standard for stibnite, because in the external standard USGS MASS-1, the Sb content is too low (about 60 ± 9 ppm) and, at the same time, Sb is highly volatile. As a consequence, the extrapolation of the data to a content of about 71 wt% when data calculation, causes a greater error than the unstable of S. At the same time, the S content in stibnite is similar to the S values in the MASS-1 standard, which is very good. In some cases, normalization of up to 100% of the total number of components was performed using traditional methods (Longerich et al., 1996). The list of determined isotopes are: ^{34}S, ^{51}V, ^{53}Cr, ^{55}Mn, ^{57}Fe, ^{59}Co, ^{60}Ni, ^{65}Cu, ^{66}Zn, ^{69}Ga, ^{72}Ge, ^{75}As, ^{77}Se, ^{95}Mo, ^{103}Rh, ^{105}Pd, ^{107}Ag, ^{111}Cd, ^{115}In, ^{118}Sn, ^{121}Sb, ^{125}Te, ^{182}W, ^{193}Ir, ^{195}Pt, ^{197}Au, ^{202}Hg, ^{205}Tl, ^{208}Pb, ^{209}Bi.

Due to polyatomic interferences with $^{40}Ar + {}^{32}S$ and $^{56}Fe + {}^{16}O$, ^{72}Ge values are conditional.

4. Results

4.1. Mineral paragenesis of the Olympiada gold deposit

About 50 minerals (sulfides, sulfosalts, stibnides, sulfoarsenides, sulfostibnides, tellurides, native elements, etc.) were recognized in the ores, among which pyrrhotite, arsenopyrite, pyrite, stibnite, and

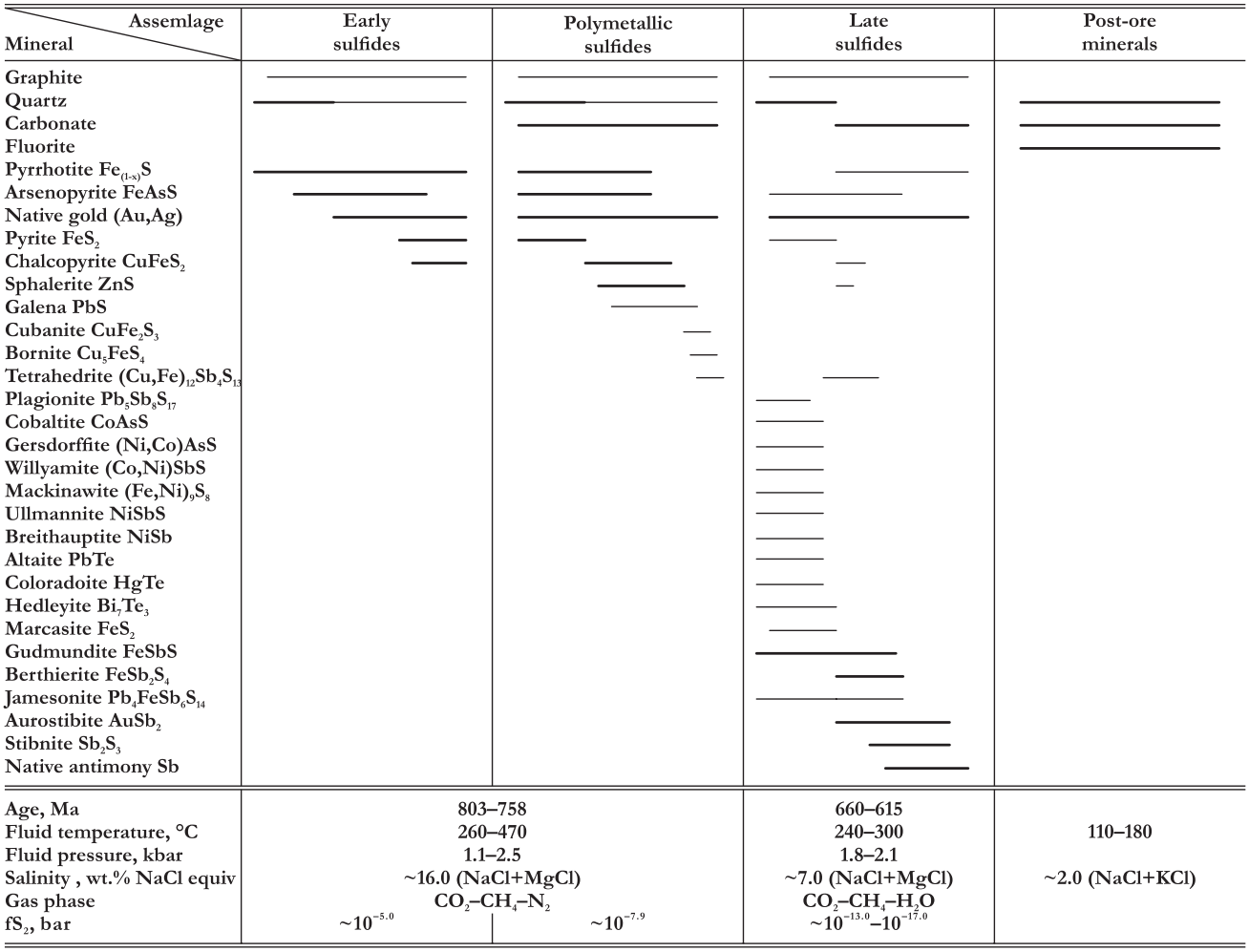

Fig. 4. Paragenesis of the mineralization at Olympiada gold deposit, compiled by A.M. Sazonov and S.A. Silyanov. Age and *PTX* parameters after (Gibsher et al., 2019a, b; Sazonov et al., 2019b; Sazonov et al., 2020).

berthierite prevail (Table A.2). Ore minerals occur in the form of oriented disseminations of granular aggregates located along cleavage fractures, schistosity and banding of rocks. There are also vein, pocket-like and massive (homogeneous) accretions several millimeters to several centimeters thick and above, as well as ore breccia.

A number of minerals have been identified in the deposit, which correspond to the different stages of hydrothermal activity of the ore system separated by tectonic breaks (Fig. 4).

The early disseminated sulfide complex of gold-arsenic ores is represented by fine acicular arsenopyrite-I, pyrrhotite-I of the early sulfides stage and a later stage of overprinted mineralization of base-metal sulfides (sphalerite-I, chalcopyrite-II, galena, etc.). The paragenesis of the early sulfide stage is represented by the predominant acicular arsenopyrite-I and pyrrhotite-I with subordinate amounts of pyrite-I and chalcopyrite-I. The mineral composition of the stage of base-metal sulfides is characterized by the development of recrystallized prismatic arsenopyrite-II, pyrrhotite-II, pyrite-II, smaller amounts of chalcopyrite-II, sphalerite-I and rare galena, cubanite, bornite, and tetrahedrite-I.

Arsenopyrite-I occurs as scattered fine acicular crystals (several μm to 1.5 mm in length) as disseminations among the main mica-quartz-calcite ore material (Fig. 5). When mineralization of the polymetallic sulfide stage is implemented arsenopyrite was recrystallized and formed long and short prismatic grains (arsenopyrite-II). The process of recrystallization of early sulfides also leads to native gold precipitation. The content of arsenopyrite varies from 0.1 to 5.0%, averaging 1.0 to 1.5%. The arsenopyrite typically forms agglomerations with pyrrhotite in the form of skeletal crystals with pyrrhotite inclusions, sometimes in growth zones and pyramids. Pyrrhotite is widespread in regular and low-grade ores as well as outside ore-bearing areas (up to 1.5–3.0%). This mineral forms fine disseminations, strip-like accretions of coarse-grained aggregates and solid coarse-grained growths confined to the coarse crystal quartz segregations.

Visible gold is noted in single cases, commonly where there is a combination of the early arsenopyrite and later polymetallic sulfides mineralization in the form of micron sized inclusions in pyrite, pyrrhotite, arsenopyrite, as well as aggregates up to 10–30 μm in size in fractures and on the surfaces of grains.

Gold-arsenic mineralization was formed in the period of 803–758 Ma by heterogeneous fluids at a temperature of 260–470 °C and pressure of 1.1–2.5 kbar. The fluid was characterized by increased salinity of ~ 16.0 wt% NaCl-eq. (NaCl + MgCl), with CO_2-CH_4-N_2 dominating the gas phase (Gibsher et al., 2019a, b; Sazonov et al., 2019b; Sazonov et al., 2020).

The late gold-antimony (stage of late sulfides) association occurs with a significant break and is overprinted by the parageneses of early associations. Mineralization of the complex is developed mainly in the

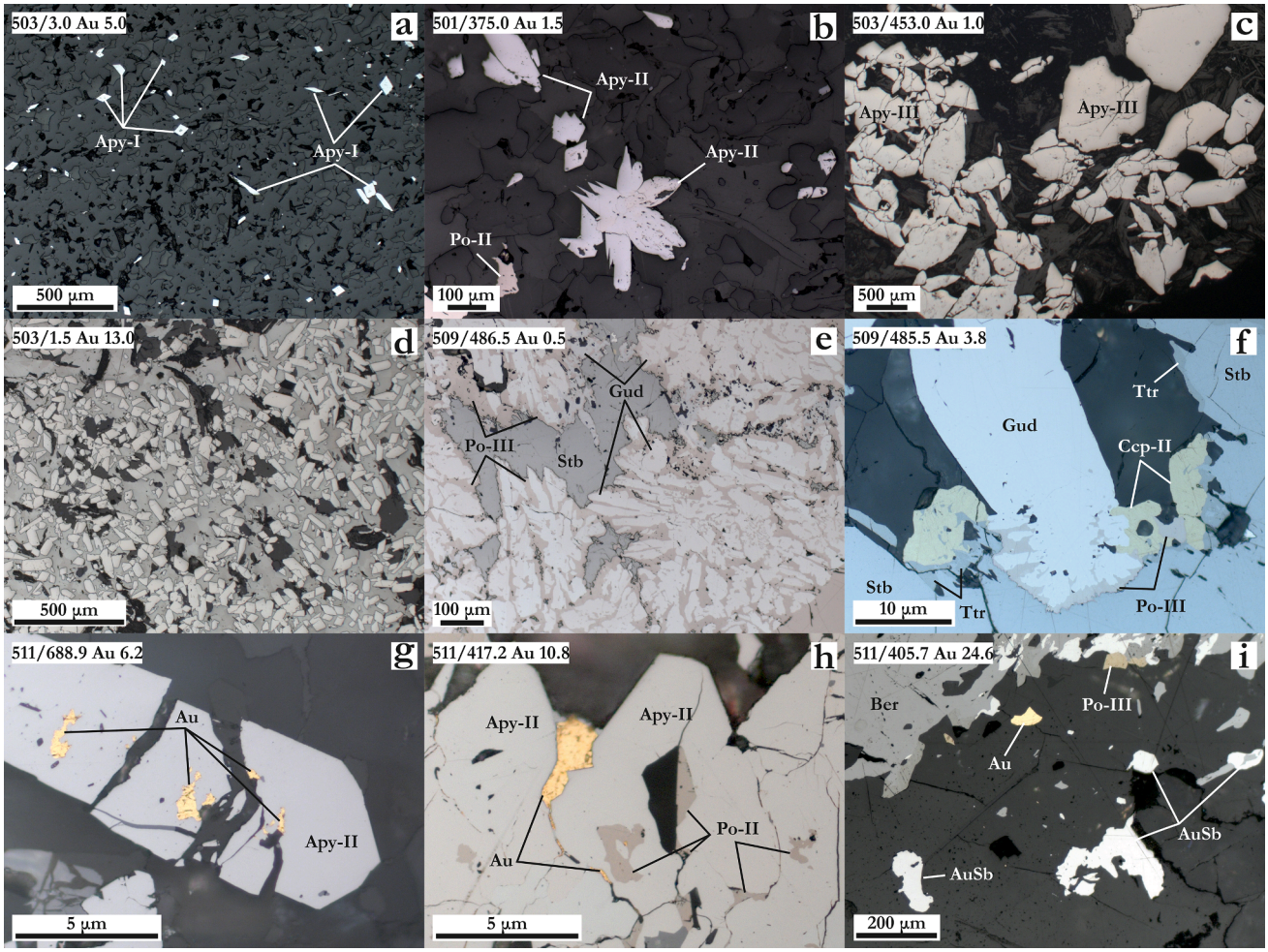

Fig. 5. Associations of ore minerals and gold (Sazonov et al., 2020): a — acicular crystals of early arsenopyrite (Apy) in quartz-carbonate mass; b — recrystallized arsenopyrite; c — coarse-grained late arsenopyrite; d — numerous acicular crystals of arsenopyrite cemented by stibnite aggregate; e — symplectite aggregate of pyrrhotite (Po) and gudmundite (Gud) in association with stibnite (Stb); f — pyrrhotite, chalcopyrite (Ccp) and tetrahedrite (Ttr) along the contact of gudmundite with stibnite; g — cataclastic crystal of prismatic arsenopyrite in quartz-carbonate matrix, gold (Au) inclusions and fracture fillings in arsenopyrite; h — gold in intergranular space and fractures in arsenopyrite and pyrrhotite aggregate; i — gold and aurostibite (AuSb) in association with berthierite (Ber). 509/485.5 Au 16.8 — sample numbers (drill hole/depth), gold grade in g/t.

Southern block of the Eastern Olympiada in the Medvezhy fault zone. Ore textures are disseminated-veinlet, pocket-like, breccia, with frequent massive homogeneous antimony minerals and coarser visible native gold and aurostibite $AuSb_2$ (Fig. 5). Arsenopyrite-III is recrystallized and has dipyramidal or short-prism morphology (up to 5 mm across) with increased Sb concentrations (wt. %) up to 1.02%; Co up to 2.96%; and Ni up to 0.74%. Pyrrhotite-III is also developed here in significant quantities, which is found in association with both Ni-Co and antimony minerals. Pyrite III was found much less frequently in the form of separate grains, as well as chalcopyrite III and sphalerite II.

The mineralogy of the complex is extremely diverse (Fig. 4) and is characterized by the development of symplectic, reaction and marginal structures (Fig. 5). The initial period of this stage formation is characterized by the deposition paragenesis of Ni-Co minerals and tellurides (ullmannite NiSbS, gersdorffite NiAsS, altaite PbTe, hedleyite Bi_7Te_3, etc.). This mineralization is characterized by the presence of small grains and marginal rims of gersdorffite and ullmannite on grains and aggregates of pyrrhotite-II and the formation of ullmannite-pyrrhotite simplicities. This is the most diverse and abundant mineral association of the deposit, but in terms of scale it occupies a subordinate position. According to our long-term observations, traces of this mineralization are observed at many gold deposits of the Yenisei Ridge, but it is widespread only at some deposits (Olympiada, Poputninsky, Veduga).

The final period of the late sulfides stage corresponds to crystallization paragenesis of antimony minerals: stibnite, berthierite, gudmundite, native antimony and subordinate tetrahedrite-II, and jamesonite (Fig. 4). The development of this mineralization occurred in a narrow temperature interval with a general reduction of sulfur fugacity to minimum values in the following generalized sequence: berthierite → stibnite → native antimony. Gudmundite occurs in several associations: idiomorphic crystals; symplectite accretions with tetrahedrite and chalcopyrite; symplectites of gudmundite-pyrrhotite composition at the boundaries of berthierite, which suggests its several origins. The interrelations of the stage minerals, as a whole, do not rule out the reactive nature of formation of some of them.

Microscopically visible (up to 70–120 μm) gold is most frequently observed in this association in the form of fractured and pocket-like accretions, as well as inclusions and aggregates with antimony and telluride minerals. Aurostibite is also present but in subordinate amount, mainly in association with stibnite, berthierite, sulfostibnides, carbonates and late quartz.

The gold-antimony association occurred 660–615 Ma ago and due to the circulation of a heterogeneous medium-temperature (240–300 °C) fluid with a pressure of 1.8–2.1 kbar. The salinity of the solution did not exceed 7.0 wt% NaCl-eq. (NaCl + MgCl), with a gas phase dominated by CO_2-CH_4-H_2O (Gibsher et al., 2019a, b; Sazonov et al., 2019b; Sazonov et al., 2020).

The post-ore veinlet fluorite-carbonate mineral group is widely developed within the ore field, but its intensity is low (Sazonov et al., 2019b; Sazonov et al., 2020).

As mentioned above, the total amount of sulfides in ores varies from 2 to 7%. The proportion of sulfide minerals in different types of ores (Au-As and Au-Sb) is different (Table 1). Both types of ores are dominated by pyrrhotite (0.5–4.0%), arsenopyrite (0.1–2.6%), and pyrite (0.1–2.1%); however, in the Au-Sb ores, the proportion of antimony minerals significantly increases (stibnite and berthierite up to 0.3–2.5%), sulfides of base metals, Ni-Co minerals and tellurides, with a much lower their amount in Au-As ores (Table 1).

Given the wide variety of sulfide minerals, as well as their different amounts in different types of ores, it is difficult to establish the exact percentage of each of them. Based on PJSC Polyus and Sovmen et al., 2009 data, as well as our mineralogical observations, the table shows the percentage of major sulfide minerals in different types of ores.

Table 1
Amount of the main ore minerals in sulfide ores of Olympiada deposit*.

Mineral	Average amount (wt. %)	
	Au-As ore	Au-Sb ore
Pyrrhotite	~2.3 (<0.5–4.0)	~1.6 (<0.1–2.0)
Arsenopyrite	~1.4 (<0.1–2.6)	~0.8 (<0.1–1.2)
Pyrite	~0.8 (<0.1–2.1)	~0.9 (<0.1–1.0)
Base-metal sulfides:	~0.01	~0.05
Chalcopyrite	*prevail*	*prevail*
Sphalerite	*subordinate*	*subordinate*
Galena	*subordinate*	*subordinate*
Antimony sulfides:	~0.1 (<0.1–0.4)	~0.7 (<0.3–2.5)
Stibnite	*prevail*	*~0.5*
Berthierite	*subordinate*	*~0.2*
Gudmundite	*traces*	*<0.01*
Antimony sulfosalts	Traces	<0.01
Ni-Co minerals and tellurides	Traces	<0.01
Minerals of Au (Au, Au(Ag, Hg), $AuSb_2$)	Traces (Au ~ 3.9 g/t)	Traces (Au ~ 2.9 g/t)
Total	~4.6	~4.1

* According to PJSC Polyus and Sovmen et al., 2009 data, with additions of authors.

4.2. Trace element geochemistry

200 LA-ICP-MS analyses were performed to study the distribution of trace elements in ore minerals of the Olympiada deposit. Some of the elements analyzed occurring in significant concentrations in most minerals: Co, Ni, Cu, Zn, As, Se, Ag, Sb, Te, Au, Pb, and Bi. Others are noted only in some minerals that have "affinity" with this element, such as Mn, Ga, In, Hg in sphalerite. The grades of some elements (Cr, Rh, Pd, Ir, Pt) were below the detection limit in all analyses. Judging by the smooth nature of the elements signal in the LA-ICP-MS curves, most of the trace elements are isomorphously distributed in the minerals, but the presence of few intensive peaks does not rule out the probability of the presence of some of them in the form of nano- and microinclusions (Fig. 6). The results are presented in Table A.3.

4.2.1. Pyrrhotite $Fe_{1-x}S$

Twenty-five spot analyses of pyrrhotite of the early sulfides stage (8 analyses), polymetallic sulfides (13 analyses) and late sulfides (4 analyses) were performed. The studied pyrrhotite is characterized by a continuous chemical composition with insignificant prevalence of S (Fe/S = 0.87–0.88).

The pyrrhotite is characterized by a minimum amount of trace elements. Only Co and Ni are present in almost all analyses (~0.4–393 and ~ 15–1,135 ppm, respectively). About a half of the analyses showed insignificant concentrations of Sb (up to 12.0 ppm) and Pb (up to 6.5 ppm).

The Co and Ni grades show the general trend of depletion from early to late generations of the mineral, while the Co/Ni ratio remains approximately at the same level (~0.5). No regularities are noted in the distribution of other trace elements. Such a limited set of trace elements (mainly Co, Ni, Se), as well as low Au concentrations are typical for pyrrhotite of gold deposits (Thomas et al., 2011; Belousov et al., 2016; Xu et al., 2020b).

4.2.2. Arsenopyrite FeAsS

Three generations of arsenopyrite (see Section 4.1) have been identified at the deposit — early acicular, late prismatic and dipyramidal. In total, 44 spot analyses of the mineral were performed (20 for acicular, 9 for prismatic, and 15 for dipyramidal). Moreover, traverses were made on three grains of dipyramidal arsenopyrite. Scanning along the profile and mapping were not performed for needle-like and prismatic arsenopyrites due to the small size of their grains.

The studied arsenopyrite are characterized by strong variations in S and As contents. The tendency of reducing the share of S and increasing

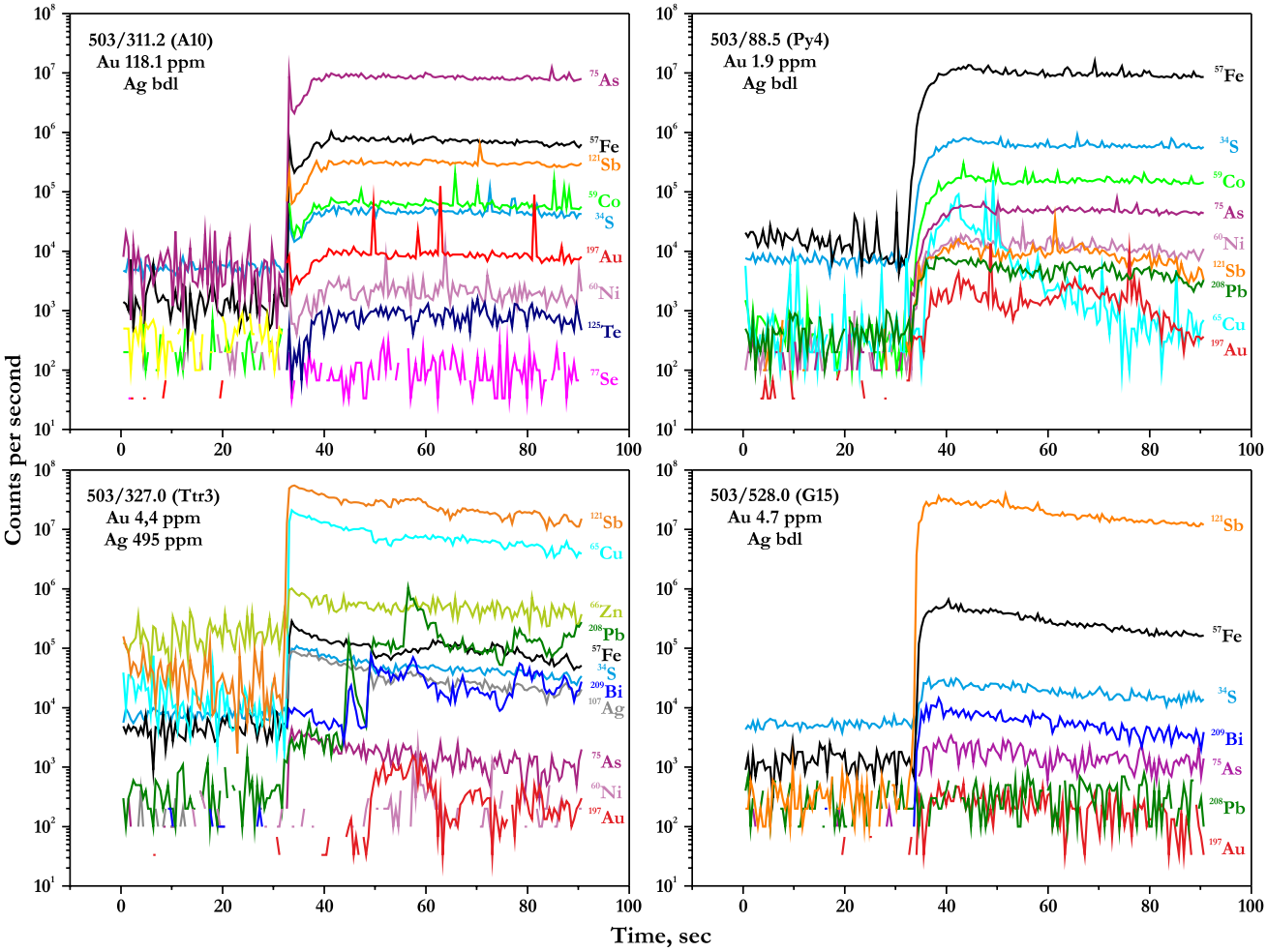

Fig. 6. Representative time-resolved LA-ICP-MS depth profiles for arsenopyrite (A10), pyrite (Py4), tetrahedrite (Ttr3) and gudmundite (G15) of the Olympiada gold deposit. 503/311.2 (A10) – sample numbers (drill hole/depth), analysis number (see Table A.3).

As is observed from early acicular (S/As = 1.12) to later recrystallized prismatic (S/As = 1.06) and dipyramidal (S/As = 0.98) varieties (Table A.4, Fig. B.1). In terms of the ratio of cations and anions, all arsenopyrites are close to stoichiometry ((S + As)/Fe = 1.95–2.16).

The following trace elements are above detection limits in most analyses and vary between, ppm: Co ~ 1–4,620; Ni ~ 39–455; Sb ~ 1,160–10,050; Te ~ 6.7–379; Au ~ 0.07–1,512; Pb ~ 0.5–50; and Bi ~ 0.3–10. The following were detected in approximately half of the analyses, ppm: V up to 4.3; Se up to 127; Mo up to 7.4; and W up to 15.4. The smooth ^{197}Au signal on the LA-ICP-MS curves indicates the state of the metal in a structurally bonded form, but in some samples the presence of peaks and the saw-cut like nature of profiles is established, which may indicate the presence of Au^0 nano-inclusions (Fig. 6) (Sung et al., 2009; Gregory et al., 2015). Also in single cases, correlating peaks of the ^{197}Au, ^{208}Pb and ^{209}Bi signal are observed, which together with the positive trend in the distribution of these elements may suggest the inclusion of Au-Bi-Pb alloys or a native gold with Pb-Bi sulfosalts.

The LA-ICP-MS traverses across the grains of prismatic and dipyramidal arsenopyrites do not establish the presence of any zoning in the distribution of trace elements, which may be associated with the alignment of the inhomogeneous chemical composition during the ore metamorphism and recrystallization of the mineral.

Reduction of the V, W, Au, Pb, and Bi concentration was identified from early to late arsenopyrite. Se was found in acicular and dipyramidal arsenopyrite, and its concentrations in acicular arsenopyrite are much higher than those in recrystallized arsenopyrite. Co and Te demonstrate the same accumulation levels in all mineral generations. Minimal Ni concentrations are typical for prismatic arsenopyrite, and maximal concentrations are typical for acicular arsenopyrite, while dipyramidal arsenopyrite takes the middle position. Sb demonstrates the trend of increasing grade from early to late arsenopyrites. Direct trend between W and V, Te and Se, Pb and Ni, Bi and Ni, Bi and W and inverse trend between Sb and Ni are characteristic.

4.2.3. *Pyrite FeS_2*

For pyrite generations from the deposit 21 point analyses were performed (10 for pyrite I, 7 for pyrite II and 4 for pyrite III), and 2 traverses for euhedral pyrite II. The chemical composition of the mineral is stable for all generations and is close to stoichiometry (S/Fe = 1.96–2.03).

Typical trace elements include, ppm: Co ~ 4.7–512; Ni ~ 7.2–5,750; As ~ 6.2–2,340 and Sb ~ 0.1–111. Approximately half of the analyses showed, ppm: V up to 3; Cu up to 122; Ge up to 3; Se up to 145; Mo up to 2; Ag up to 1.4; Te up to 40; W up to 1.2; Au up to 2; Pb up to 33; and Bi up to 2.6. Flat LA-ICP-MS patter indicate that most of the elements are isomorphically distributed in the mineral structure, but in single cases the presence of Au and sulfosalt (As-Sb-Pb-Cu) inclusions can be assumed (Fig. 6).

Profiles for two grains of euhedral pyrite II show weak zoning in the distribution of As, Co, Sb, Ni, Bi, expressed in depletion of the periphery with arsenic grains and their enrichment with Co, Sb, Ni, and Bi.

In the Se, Sb, Te, and Pb distribution, the tendency is for their concentration to decrease from early to late mineral generations. The As, Ge, Au and Bi concentrations are approximately at the same level in all generations. The Au grade is about 0.6 ppm on average and decreases

from early to late generations. Ag appears only in pyrites of the first two stages, with a weak tendency to increase in pyrite II.

Early pyrite is significantly depleted in both Co and Ni, with the Co/Ni ratio usually < 1. Pyrite II is characterized by an increase in the amount of Co by approximately an order of magnitude, while Ni remains at approximately the same level (Co/Ni 2.9–19.5). The Co content in pyrite III remains at the level of pyrite II, but here the amount of Ni increases by approximately an order of magnitude, which leads to a decrease in the Co/Ni ratio to the pyrite I levels. The increase in the Co content in pyrite II may be related to the simultaneous formation of pyrrhotite, which accumulated mainly Ni (Conn et al., 2019).

A part of trace elements (Co, Ni, Cu, Zn, Hg, Pb, Bi) probably replaces Fe^{2+} in the mineral structure (Dehnavi et al., 2018; Voute et al., 2019). At the same time, a weak negative trend between S and As indicates a preferred substitution as per As → S type and the formation of the mineral in reducing medium (Keith et al., 2018).

4.2.4. Sphalerite ZnS

We carried out 11 point analyses of sphalerite (2 for sphalerite I and 9 for sphalerite II). Sphalerite is one of the few minerals that concentrate a large amount of trace elements. In terms of the S content, the mineral is close to stoichiometry (S 32.21–33.48 wt% SEM EDS).

In most analyses, significant ppm concentrations of the following elements were noted: Mn ~ 87.7–337.3; Fe ~ 28,000–67,600; Co ~ 0.4–74.7; Cu ~ 30.8–194; Ga ~ 0.5–2.1; As ~ 0.6–52; Ag ~ 0.2–1.2; Cd ~ 68.5–532; In ~ 1.1–32.6; Sn ~ 0.4–1.8; Sb ~ 2.8–174.3; Au ~ 0.02–0.20; Hg ~ 282.6–1,690; and Pb ~ 0.4–17.2. Approximately a half of the analyses also showed, ppm: Se up to 166.5; Te up to 1.1; and Bi up to 2.20. Inhomogeneity in the distribution of Cu is noted, which is reflected in the presence of single peaks, as well as fluctuations in the content depending on the depth of ablation. This may be due to the presence of chalcopyrite microinclusions in the mineral.

Sphalerite of the polymetallic sulfides stage is characterized by Mn and Hg predominance, while sphalerite of stage III is enriched with Co, Ni, Se, Sn, Sb, Au, Pb, and Bi. Ag, Cu, Ga, Ge, As, Cd and In are present approximately at the same level in both mineral generations. Negative trend between Zn and Fe, Cd, In, Hg, and Cu and positive trend in the Mn-Hg, Au-Cu, Ag-Ga, and Ag-Sn pairs are characteristic. The observed trends agree well with the abundance of variants of isomorphic substitution in a mineral, and it is assumed that most of the trace elements are "dissolved" in its lattice (Cook et al. 2009, Murakami & Ishihara, 2013; Belissont et al., 2014; Lee et al., 2019b; Wei et al., 2019; Zhuang et al., 2019; Xu et al., 2020a).

4.2.5. Chalcopyrite $CuFeS_2$

Due to the limited distribution and small size of grains, only 8 spot analyses of chalcopyrite were performed (4 analyses of chalcopyrite at the polymetallic sulfide stage and 1 analysis at the late sulfide stage). The chemical composition of the mineral varies within a narrow range, approaching stoichiometry (SEM EDS), wt. %: Cu – 34.44; Fe – 30.84; S – 34.53.

The most common trace elements noted, ppm: In ~ 0.8–9.2; Sn ~ 12.7–76.2 and Sb ~ 11.5–103. Half of the analyses had the following elements above detection limits, ppm: Mn up to 362; Ni up to 11.6; Zn up to 439; As up to 4.3; Ag up to 3.3; Pb up to 15.6; and Bi up to 1.4. Trace elements are present both in the form of a solid solution in the mineral structure (e.g., Sn, In, Zn) and in the form of nanoinclusions, and zoning in depth is additionally noted in the distribution of some elements.

The volume of the available data shows enrichment of chalcopyrite I with Mn, Ni, Zn, As, Ag, Sb, Pb, while late chalcopyrite II mainly concentrates In and Sn. As compared to co-existing sphalerite, chalcopyrite is insignificantly enriched in Ag and Sn, but it is depleted in Cd and In, which agrees well with earlier published data on elements redistribution between minerals (Xu et al., 2020a). It has been demonstrated that chalcopyrite crystallizing together with other polymetallic sulfides (e.g., sphalerite and galena) is prone to low concentrations of almost all trace elements, which probably also takes place at the Olympiada deposit (George et al., 2018).

4.2.6. Ullmannite NiSbS

It is a rather rare mineral in the deposit, usually forming small size of grains, therefore only six point analyses were performed in one specimen. The chemical composition of ullmannite is close to stoichiometry in terms of S and Sb (S ~ 14.68 wt% and Sb ~ 58.8 wt% SEM EDS). At the same time, we found a strong variation in the content of Ni and Co — Ni 15.7–24.6 wt% and Co 3.8–14.5 wt% (SEM EDS).

The mineral is characterized by a limited set of trace elements, the most common being As (~72–248 ppm) and Bi (~806–1,206 ppm). Almost all trace elements are characterized by an even nature of the signal in the LA-ICP-MS curves, except for lead, for which there is a "step" change in the grade in some analyses.

The first data on the distribution of trace elements in ullmannite is given in this paper. However, due to the small analytical selection, only the main type of chemical trends can be specified: the mineral is characterized by wide isomorphism between Co and Ni; main trace elements are As and Bi; As is assumed to replace S in the mineral structure, while Bi takes the position of Ni.

4.2.7. Tetrahedrite $Cu_{12}Sb_4S_{13}$

Eight spot analyses of tetrahedrite were carried out, which, on the basis of a permanent association with antimony minerals, is attributed to stage III. The main components of the mineral show no significant variations (Cu 37.3–38.3; Sb 30.3–30.8; S 24.3–24.8 wt%), except for Fe and Zn, whose contents vary between 3.2 and 5.5 and 2.3–8.5 wt%, respectively (SEM EDS).

The mineral conistantly contains the following elements above detection limits, ppm: Mn ~ 5.4–159; Co ~ 0.8–31; As ~ 41.1–300; Se ~ 22.3–56; Ag ~ 348.8–3,811; Cd ~ 8.8–91.6; In ~ 0.1–4.3; Hg ~ 62.3–868; Pb ~ 2.0–1,820; and Bi ~ 0.2–442.

Tetrahedrite in association with sphalerite, pyrrhotite, berthierite and jamesonite is characterized by maximum concentrations of Cd and Hg and minimum concentrations of As and Ag. Tetrahedrite in the same association, but without pyrrhotite, shows maximum concentrations of As, Se, and Ag, but minimum concentrations of Mn, Cd, Pb, and Bi. If, instead of pyrrhotite, native antimony occurs in the association, the maximum concentrations are typical for Mn, Co, Ni, Te, Pb, and Bi (also Au are noted only here), and the minimum concentrations are typical for Se and Hg.

A weak positive trend between Ag and As was noted. Previously it was assumed that Ag and As were incompatible in tetrahedrite (Ebel and Sack, 1991), but Zhang et al. showed that coherent accumulation of elements in a mineral is possible due to their concentration in a hydrothermal solution at a later stage (Zhang et al., 2020). Therefore, the most Ag-enriched tetrahedrites should correspond to the final stage of mineralization formation.

The mineral is also characterized by the correlation of Bi, Pb, Au and, to a lesser extent, Ni peaks in the LA-ICP-MS curves, while other elements (Ag and As primarily) do not show such a tendency (Fig. 6).

4.2.8. Berthierite $FeSb_2S_4$

Nineteen spot analyses of the berthierite composition at the deposit were performed. The chemical composition of the mineral is characterized by high stoichiometry; the content of the main components is on average (SEM EDS), wt. %: S – 30.1; Sb – 57.0; and Fe – 12.5.

The mineral is enriched with a large number of trace elements, among which the most common are, ppm: Mn ~ 113.6–7,722; Co ~ 0.2–440; Ni ~ 0.9–299; Cu ~ 1.1–90; As ~ 7.4–2,001; Se ~ 3.7–1,002; Ag ~ 0.03–2.30; Cd ~ 0.3–29; In ~ 0.2–8; Sn ~ 1–14; Te ~ 1.2–16.5; Pb ~ 606.7–4,310; and Bi ~ 1.7–632. Approximately a half of the cases showed the following elements above detection limits, ppm: Zn up to 605; Hg up to 33 and Tl up to 0.20.

The studied mineral grains are characterized by three main

associations: berthierite; berthierite + native antimony; berthierite + jamesonite ± pyrrhotite and ullmannite. Jamesonite is usually present in the form of submicron elongated inclusions in berthierite, confined to the boundaries of pressure twins, which can be interpreted as the breakdown of berthierite originally enriched with lead into berthierite + jamesonite. In, Cd, Pb and Bi are the most contrasting in the identified associations. Thus, pure berthierite, which seems to be the earliest, is characterized by minimal amounts of Cd and In, as well as Pb and Bi. Berthierite in association with jamesonite (later than pure berthierite) shows high levels of Cd and In as well as maximum levels of Pb and Bi. There are two analyses of berthierite in association with jamesonite and native antimony, which are characterized by the maximum content of In and Bi. The association of berthierite and native antimony is the latest and has maximum levels of Cd and In, while Pb and Bi are at the level of pure berthierite.

4.2.9. Stibnite Sb_2S_3

Twenty-two stibnite analyses were performed. All mineral grains are characterized by high stoichiometry (Sb ~ 71.3 wt%; S ~ 28.1 wt% SEM EDS).

As compared to berthierite, stibnite differs in much smaller amount of trace elements, ppm: Cu ~ 17.5–120; Se ~ 107–2,554; Ag ~ 0.2–2; Sn ~ 0.5–7.9; Te ~ 3.4–124; Pb ~ 127.4–505; and Bi ~ 0.3–2.2.

Stibnite is also found in several other associations: in the form of independent accretions; stibnite + berthierite; stibnite + berthierite + jamesonite; stibnite + native antimony. However, no regularities in the distribution of trace elements in stibnite of different associations have been revealed. The mineral is also characterized by a lack of regularities in the distribution of trace elements, except for Se and Te, which show a positive relationship, and Pb and Cu with a strong positive correlation ($r^2 = 0.85$).

4.2.10. Gudmundite FeSbS

The deposit has several gudmundite growths within the late sulfide stage (see Section 4.1). Some of them were developed as a result of the reaction of sulfides already formed or during their decomposition. Such gudmundite growths are characterized by complex symplectite structures and small size, which does not allow their analysis with the LA-ICP-MS method. On the contrary, euhedral gudmundite occurs as coarse (up to 1 mm) crystals and does not form complex aggregates with other minerals, thereby allowing 13 spot analyses as well as one profile.

While its composition is close to stoichiometry (Fe 25.9; Sb 58.1; S 15.5 wt% SEM EDS), the mineral is characterized by a limited set of trace elements, ppm: Cu ~ 7.3–171; Zn ~ 10–190; As ~ 9.1–692; Au ~ 0.2–4.7; Pb ~ 1.5–63, and Bi ~ 0.5–71.

The profile along one of the mineral grains shows complex zoning in the distribution of As, Ni, Co, Te and, to a lesser extent, Au (Fig. B.2). However, high grades of Bi, Ni, Co, Te, and Au are typical for the same areas, while As demonstrates an opposite trend. Gudmundite is the only mineral of the late sulfides stage that contains higher (>1 ppm) Au concentrations (Fig. 6).

Since only one type of mineral was analyzed, the distribution of trace elements does not show any significant variations. The differences formed as a result of reaction processes probably have a different microelement composition, but this requires further investigation.

4.2.11. Jamesonite $Pb_4FeSb_6S_{14}$

Six analyses of jamesonite from the deposit were carried out. The average chemical composition of the analyzed grains corresponds to (SEM EDS), wt. %: Sb – 35.8; Pb – 41.1; S – 20.7; and Fe – 2.6. The mineral is characterized by an admixture of a large number of trace elements, ppm: Mn ~ 154.7–1,168; Co ~ 0.4–22.1; Cu ~ 1.3–68.7; Zn ~ 17.2–33.6; As ~ 5.0–206; Se ~ 35–173; Ag ~ 0.1–7.7; Cd ~ 4.6–51; In ~ 0.8–7.8; Sn ~ 11.2–31.4; Te ~ 364–882; Au ~ 0.03–0.40; Tl ~ 0.3–1.1; and Bi ~ 91.5–3,262.

Jamesonite were analyzed in two different associations: jamesonite + berthierite + native antimony and jamesonite + pyrrhotite + ullmannite. The trace element composition of the mineral varies significantly depending on its mineral association. Thus, the mineral of the first association is characterized by minimum concentrations of Mn, Co, Cd, In, Sb, Te, Au, and Bi, and maximum concentrations of Cu, Se, Ag, Sn, Hg, and Tl. Inverse regularities are typical for the mineral in association with ullmannite.

5. Discussion

5.1. Distribution of Au

At Olympiada deposit there is a tendency in the distribution of "invisible" gold to decrease its concentrations in sulfides in the trend from early to late stages, which correlates inversely with an increase in the share of free metal in the late sulfides association (Fig. 7). The main carrier mineral of "invisible" gold is early acicular arsenopyrite with 12.5–1,512.0 ppm Au. The later recrystallized varieties, such as prismatic (Au 4.3–114.0 ppm) and dipyramidal (Au 0.07–2.40 ppm) arsenopyrite, contain considerably less Au (Fig. 7). It is characteristic that analyses with the Au grade below detection limits are noted only for a dipyramidal variety of the mineral (more than half of the analyses). This also confirms the decrease of the share of Au during the mineral recrystallization.

Previous studies show similar Au grades in arsenopyrite. By INNA, ICP-MS, and atomic absorption methods, Au concentrations were determined to be from 0 to 2,130 ppm (Genkin et al., 1994; Genkin et al., 1998; Genkin et al., 2002; Novozhilov & Gavrilov, 1999; Novozhilov et al., 2014; Silyanov et al., 2021a). Spot analyzes by SIMS and EPMA methods show the following Au ranges (ppm): 0.07–2,298 and 0.03–4,700 (Genkin et al., 1998). In some of these works, it was also shown that increased Au concentrations are characteristic of acicular arsenopyrite (Novozhilov & Gavrilov, 1999; Novozhilov et al., 2014; Silyanov et al., 2021a).

Pyrite deposition, regardless of the stage, contain equally low amounts of Au ~ 0.4 ppm, whereas Au > 1 ppm concentrations are found in single cases. However, the concentration of "invisible" gold is on average higher in the mineral of the early sulfides stage (~0.6 ppm), while pyrites of later stages have a large number of analyses with the Au grade below detection limits.

Previous studies also show low Au grades in pyrite: SIMS 0.03–0.53 ppm; INNA 0–10.41 ppm; ICP-MS 0.15–2.54 ppm (Genkin et al., 1994; Genkin et al., 1998; Silyanov et al., 2021a).

The positive correlation between Au and As in pyrite has been demonstrated in many papers (Cook and Chryssoulis, 1990; Arehart et al., 1993; Pals et al., 2003; Reich et al., 2005; Benzaazoua et al., 2007; Deditius et al., 2008), but is weak in pyrite of Olympiada deposit, which is also described in the literature (Simon et al., 1999; McClenaghan et al., 2004; Reich et al., 2005; Chouinard et al., 2005; Paktunc et al., 2006; Benzaazoua et al., 2007; Gregory et al., 2016) suggesting that As is not a mandatory condition for the isomorphic incorporation of Au into the mineral structure.

The most common valence state of Au, both in natural As-pyrite and in a synthetic As-free mineral, is Au^{1+} (Simon et al., 1999; Trigub et al., 2017; Pokrovski et al., 2019; Merkulova et al., 2019), but both Au^{3+} and Au^{1-} are not excluded (Arehart et al., 1993; Simon et al., 1999; Chouinard et al., 2005). Based on the presence of weak positive trend in Au-As and Au-Cu pairs, several isomorphism variants can be assumed: joint $Fe^{2+} \rightarrow Au^{3+}$ and $S^{2-} \rightarrow As^{1-}$ or paired $2Fe^{2+} \rightarrow Au^{3+} + Cu^{+}$ substitution.

As mentioned above (see Section 4.1), the main minerals of the deposit's ores are arsenopyrite and pyrrhotite. Pyrite is significantly less common. This fact, as well as low concentrations of Au in pyrite, and the absence of Au in pyrrhotite, suggest that at the stage of early sulfides and base-metal sulfides, it is arsenopyrite that is the main concentrator of "invisible" Au.

Early acicular arsenopyrites with an increased content of "invisible"

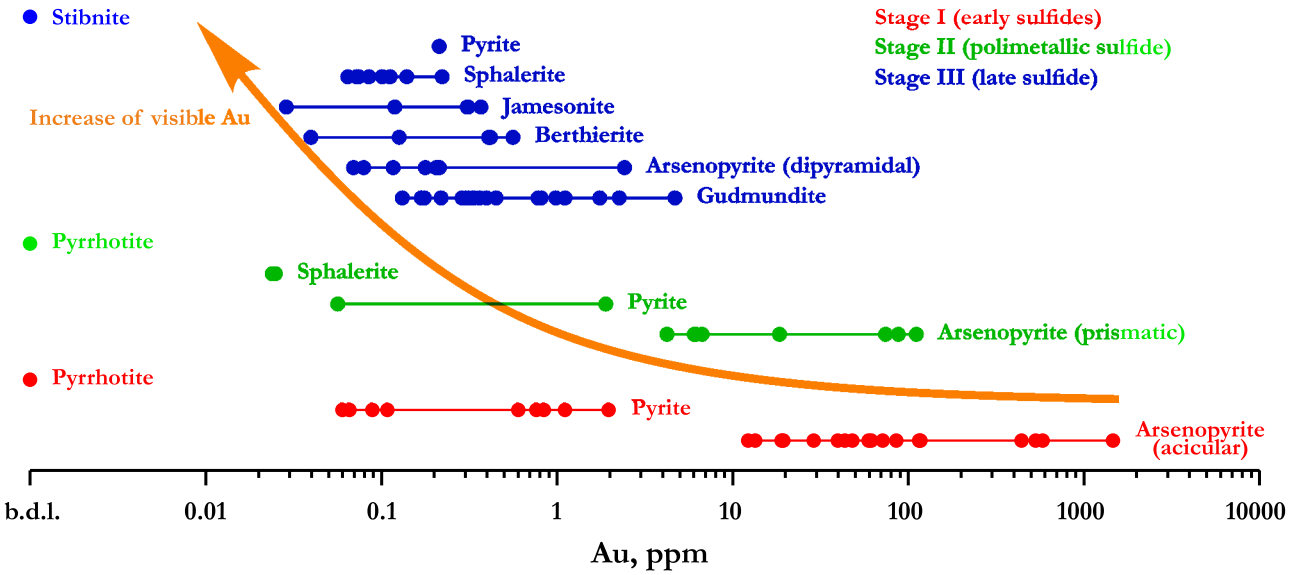

Fig. 7. Au content in sulfide minerals of the Olympiada deposit (b.d.l. – below detection limit). Quantity of free native gold sufficiently increased in the late stages of the ore-forming process.

gold on the one hand and a reduced structural and chemical stoichiometry on the other, are generally characterized by elevated formation temperatures (up to 450–500 °C) both for the Olympiada deposit and for other gold-bearing objects of the Yenisei Ridge. At the same time, late stoichiometric Au-poor varieties are formed at lower (~300–400 °C) temperatures (Sazonov et al., 2019a). This does not exclude the possibility of a decrease in the capacity of the lattice of a mineral with respect to gold with a decrease in the temperatures of its formation or recrystallization.

Most analyses of minerals of the late sulfides stage show low concentrations of Au (<1 ppm). Only gudmundite and single grains of late dipyramidal arsenopyrite contain higher Au grades. Gudmundite exhibits maximum concentrations of "invisible" gold ~ 0.9 ppm, which is about twice as high as the grade in pyrite. Obviously, such enrichment of gudmundite with "invisible" gold is due to its structure. As is known, gudmundite is completely isostructural to arsenopyrite, which, firstly, explains the constant impurity of Sb in arsenopyrite and As in gudmundite and, secondly, relatively high concentrations of Au in gudmundite. The same mechanisms for inclusion of impurity atoms in the structure may act in the case of arsenopyrite and gudmundite.

The Au grade was also determined for almost all analyses of jamesonite (0.03–0.40 ppm) and sphalerite (0.07–0.20 ppm) at this stage. Single analyses show an impurity of Au in berthierite up to 0.6 ppm and tetrahedrite up to 0.2 and 4.4 ppm. Overlap of Bi, Pb and Au peaks in the LA-ICP-MS curves of tetrahedrite may indicate the presence of inclusions of Au-Bi-Pb composition, which may have been formed as per the *hydrothermally-assisted melt-collector model* (Tooth et al., 2013; Belousov et al., 2016; Vikent'eva et al., 2018; Cave et al., 2019).

Stibnite and berthierite, some of the most abundant late sulfide minerals, contain extremely low concentrations of "invisible" Au. On the other hand, gudmundite developed in subordinate quantities contains an order of magnitude more "invisible" gold. The same tendency is shown by single analyses of arsenopyrite of this stage. This, in our opinion, suggests that the main concentrations of "invisible" gold at this stage are associated with gudmundite and, to a lesser extent, with arsenopyrite.

We have already noted that the bulk of the native gold of the deposit is confined to the stages of base-metal sulfides and late sulfides. This may indicate that at the stage of early sulfides, the fluid was unable to precipitate native gold and conditions existed for the deposition of only "invisible" Au in arsenopyrite.

According to the LA-ICP-MS patterns, most of Au in the minerals is evenly distributed and in a structurally related form. The As-Au profile with a line reflecting the limit of Au solubility in the arsenic pyrite structure also testifies to the same fact (Fig. 8) (Reich et al., 2005). This curve also indicates a general weak positive trend between Au and As in the minerals of the deposit, except for arsenopyrite.

The positive trend between Au and W, which is mainly characteristic of early stage arsenopyrite, is most distinct (Fig. 8). Weak positive trend were established for the Au-Co, Au-Ni, Au-Se, and Au-Te pairs. On the Au-Sb, Au-Pb, Au-Bi curves, the positive trend is weaker (Fig. B.3). In general, we note the possibility of identifying two trends or populations in the distribution of trace elements in sulfides of the Au-As (stage I and II) and Au-Sb (stage III) associations (Fig. 8). Moreover, there is no correlation ($r^2 = 0.001$) between Au and Ag.

In general, the Au-W-Se-Te association of the early stage may indicate a relationship with a magmatic source, but this is not always considered correct (Goldfarb et al., 2005; Goldfarb & Groves, 2015). At the same time, the association of Au with W, as well as Bi and Pb, is typical for the deposit of the *reduced intrusion-related gold systems* group, associated with acidic intrusions of the ilmenite series (Hart, 2005). However, Se and Te may also have been scavanged from metasedimentary sequences (Nekrasov, 1991). Such contradictions do not allow at present to unambiguously indicate the source of the ore matter of the deposit. However, in our opinion, the association of Au with W, as well as the general Au-Sb-W-Bi specificity of the ore field deposits (Olenye (Au-W), Vysokoe-2 (W), Titimukhta (Au-Bi)), does not confirm borrowing of these metals from metasedimentary strata.

5.1.1. *"Invisible" gold in arsenopyrite*

The data shows that "invisible" gold is concentrated mainly in early arsenopyrite, with weak negative trend between Au and As content. The data contradicts the well-established concepts which suggest Au replaces Fe in the structure of the mineral with the formation of the closest arsenic-dominated environment, which determines the positive correlation between Au and As and the negative correlation with Fe (Nekrasov, 1991; Fleet & Mumin, 1997; Benzaazoua et al., 2007; Morey et al., 2008). However, absence of direct correlation with As is also reported (Fleet & Mumin, 1997; McClenaghan et al., 2004; Lee et al., 2019a).

It is also assumed that "invisible" gold can concentrate in defects in the crystal structure of arsenopyrite, as well as accumulate on the surface of a growing crystal (Nekrasov, 1991; Kravtsova et al., 2015;

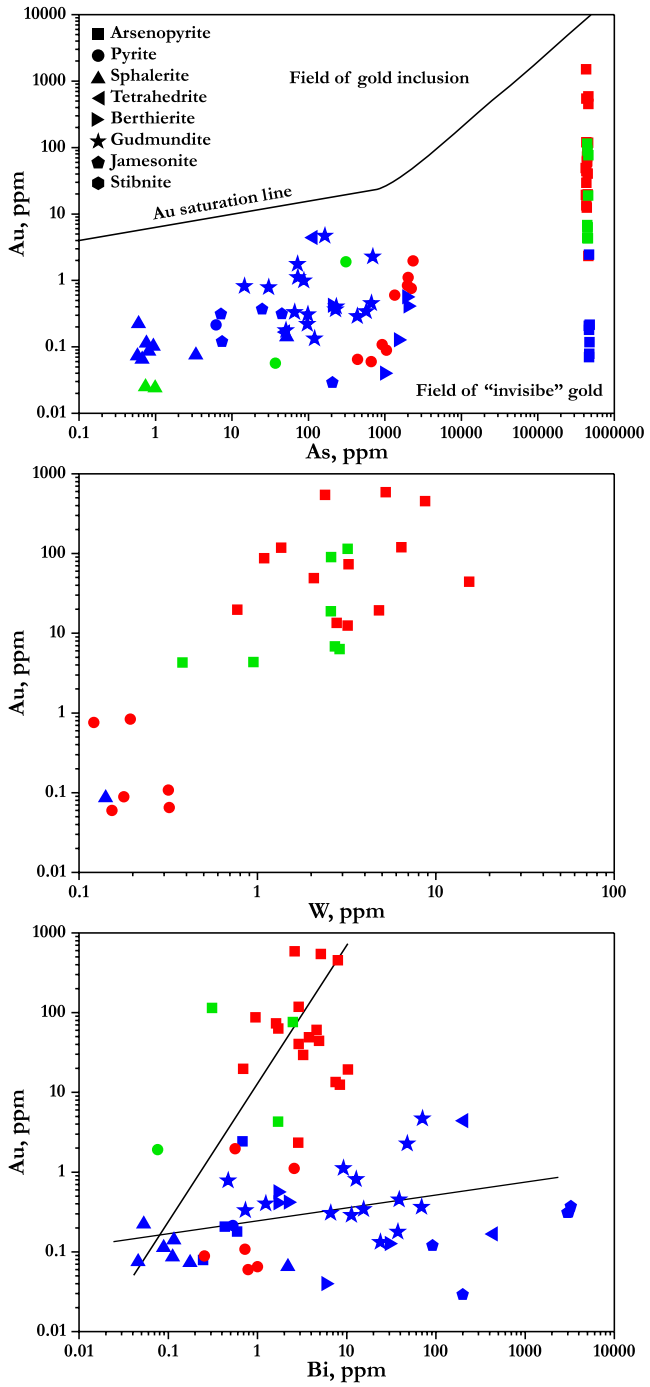

Fig. 8. Plots of the Au grade dependence on As, W and Bi. Au *vs* As diagram is according to (Reich et al., 2005).

Kravtsova et al., 2020).

The study of the interrelation between increased concentrations of "invisible" gold and the mineral composition (according to the extended selection covering the main gold deposits of the Yenisei Ridge) shows the trend of increasing amount of Au with deviation of the S/As ratio from stoichiometric values. Also, a consistent increasing grade of "invisible" gold is established for arsenopyrite of the Olympiada deposit (Fig. B.4) with a decrease in structural stoichiometry due to the different composition of the first coordination sphere around the Fe atom (Sazonov et al., 2016; Kirik et al., 2017; Sazonov et al., 2019a).

The LA-ICP-MS curves of arsenopyrite show that most of Au is in a structurally bound form, as evidenced by the even nature of the ^{197}Au signal. However, the presence of single peaks and a "saw-like" nature of the signal indicate the presence of Au^0 nanoinclusions, which is consistent with the data of the ^{197}Au Mössbauer spectroscopy, according to which up to 97% of "invisible" gold may be present in arsenopyrite of the deposit as nanoinclusions (Genkin et al., 1998).

The mechanism of inclusion of structurally bound gold in arsenopyrite remains questionable. The absence of assumed negative trend with Fe, as well as the dependence of the "invisible" gold grade on the ratio of anions do not confirm the mechanism of substitution as per Au → Fe type, but assume the connection of substitution processes with the mineral anion sublattice.

Thus, at this stage of research, it is possible to postulate that "invisible" gold in the early acicular arsenopyrite of the deposit is present both in the form of Au^0 nanoinclusions and in a structurally bound form, which does not contradict the established concepts (Boiron et al., 1989; Mumin et al., 1994; Genkin et al., 1998; Cabri et al., 2000; Palenik et al., 2004; Morey et al., 2008; Sung et al., 2009; Trigub et al., 2017; Merkulova et al., 2019). The relationship between these probably varies widely and is determined by different factors.

5.2. Distribution of Ag

Ag behaves in contrast with Au, showing the trend of enrichment of later stage minerals (Fig. 9). Tetrahedrite containing high Ag concentrations (from 348 to 3,811 ppm) in its crystal structure is most responsible for this. Moreover, we provide first data about presence in the ore deposit of argentotetrahedrite-(Fe) $(Ag_{1,84}Cu_{8,00}Fe_{1,48}Zn_{0,58})_{11,90}Sb_{4,06}S_{13,00}$ with Ag content up to 11 wt%.

Jamesonite containing low Ag concentrations (0.1–7.7 ppm). Sphalerite, stibnite and berthierite concentrate Ag at about ~ 0.6 ppm. In single cases Ag concentration are noted in gudmundite as well (0.2–0.4 ppm).

Stibnite and berthierite predominate in this association in terms of relative abundance; tetrahedrite, jamesonite, and sphalerite are present in subordinate amounts. This allows us to say that the bulk of Ag at this stage is concentrated in tetrahedrite, stibnite, and berthierite.

The highest concentration of Ag in the polymetallic sulfides stage association and chalcopyrite has concentrations of ~3.0 ppm; pyrite and sphalerite at this stage concentrate an order of magnitude less Ag. The only mineral of the early sulfides stage in which stable impurities of Ag are noted is pyrite (0.2–1.4 ppm).

The chalcopyrite is most enriched in Ag at this stage is developed in small amounts, which probably indicates its insignificant contribution to the overall Ag balance. Galena can also be a potential Ag concentrator at this stage. However, the small size of its grains, as well as the extremely low abundance in ores, did not allow for its analysis. In this regard, it can be assumed that, even at high contents, galena is unlikely to concentrate more Ag than minerals of the late sulfide stage.

The absence of Ag in arsenopyrite of all generations (except for one analysis) is typical, which is consistent with the data on the absence of correlation ($r^2 = 0.001$) between Au and Ag. The obtained data indicate that Ag played a significant role in the ores only at the stage of polymetallic sulfides – late sulfides. The data partly solves the question of the mode of Ag occurrence in the Olympiada ores, an answer that hasn't been provided since the beginning of studies of the deposit. Single publications indicate the presence of silver minerals in the ores (Bernatonis, 1999; Silyanov et al., 2021a). The presence of native silver in the ores was also reported (Li, 2003), but this was not confirmed by further research. However, according to the results obtained, most of Ag in the deposit is concentrated in the mineralization of Stage III as isomorphic admixture.

5.3. Distribution of other trace elements

As and Sb dominate the ore process in the most contrasting way. In general, it is natural that As dominated at the early stages of mineral

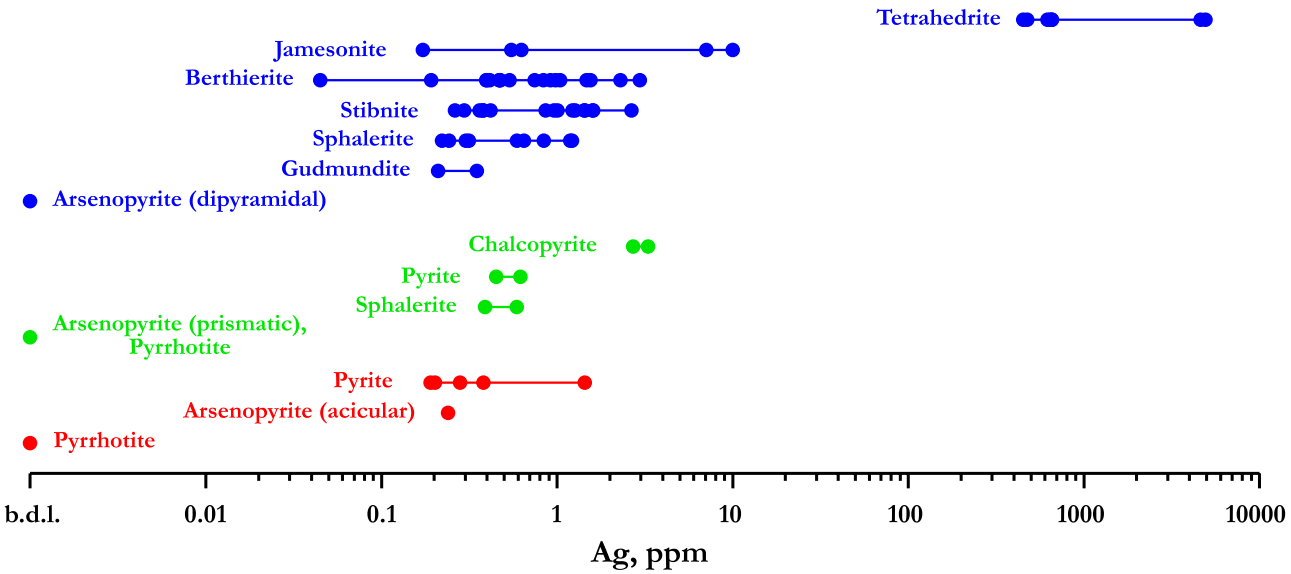

Fig. 9. Ag content in sulfide minerals of the Olympiada deposit (b.d.l. – below detection limit).

development, as the result of which most of arsenopyrite was formed (Au-As ores), but at later stages Sb was the main element controlling mineral formation (Au-Sb ores). These trends can be clearly seen in the mineralogy of the deposit (see Fig. 4). However, the analysis of the LA-ICP-MS data (diagrams shown in Fig. 10) allows us to state that Sb played an important role at the initial stages of mineral formation as well. The distribution of As is more heterogeneous, but its grades remained significant throughout the mineral formation.

Co and Ni are transitional elements at the deposit, occurring in significant quantities in almost all minerals of all mineral formation stages (Fig. 10). There is a tendency to decreasing Ni content from the stage of early sulfides to the end of the polymetallic sulfides stage and its growth at the stage of later sulfides. The exceptions are tetrahedrite, berthierite, gudmundite, and jamesonite, which have Ni at the level of early sulfides (or slightly below). The distribution of Co is more homogeneous; in general, there are approximately equal levels of accumulation at all stages of mineral formation. A decrease in Co concentrations in tetrahedrite, berthierite, gudmundite, and jamesonite, by analogy with Ni, draws attention (Fig. 10). Most analyses have the Co/Ni ratio between 0.1 and 10.0, but both higher (up to 1,000) and lower (~0.01) values are noted.

Increased concentrations of granitophile elements (Bi, Te, W), as well as As, Sb in arsenopyrite of Olympiada deposit are interpreted by some researchers as a relationship with intrusions (McFarlane et al., 2011; Augustin & Gaboury, 2019). However, there are other opinions, according to which As, Bi, Sb, Te, and W are released from hosting sedimentary rocks during metamorphism (Pitcairn et al., 2006).

Pb and Bi demonstrated tendency to concentrate in later stage minerals (for example, berthierite, tetrahedrite, gudmundite, stibnite) compared to early stage minerals (Fig. 10). Except for some anomalies (increased concentrations in early associations or on the contrary reduced concentrations in later ones, which can be explained by both crystal-chemical control and local fluctuations in the fluid composition) elements correlate directly ($r^2 = 0.7$) with each other. The most common minerals of the late sulfide stage are stibnite and berthierite, with subordinate amounts of ullmannite, tetrahedrite, gudmundite, and jamesonite. Their significant enrichment in Pb and Bi allows us to say that the main concentrations of these metals are confined to the stage of late sulfides.

Such trends, although less pronounced, are also present for Se (Fig. 10). It should be noted that its impurity is almost absent in minerals of the base-metal sulfides stage. The Te content is generally stable for the early and late sulfides associations, but, by analogy with Se, it is noticeably depleted in minerals of the base-metal sulfides stage. Probably, the mineralization of the stage of base-metal sulfides is the most depleted in these elements, since the most common minerals either contain small amounts of these elements or do not contain them at all. At the same time, the main minerals of the early sulfide stage (arsenopyrite and, to a lesser extent, pyrite), as well as the late sulfide stage (arsenopyrite, berthierite, and stibnite) contain approximately the same amount of Se and Te. Based on this, the fluid that formed these associations contained approximately the same amount of Se and Te.

The strong bond in the Pb-Cu pair in stibnite indicates a coherent accumulation of elements, probably due to crystal-chemical factors, namely, pair substitution of $Cu^{+}+Pb^{2+}\leftrightarrow Sb^{3+}$, which was also demonstrated for the Woxi Sb-Au-W deposit (China) (Fu et al., 2020). A positive relationship between Se and Te was also detected for stibnite of the Woxi deposit, but the content of these elements is rather low, in contrast to their concentrations in the Olympiada mineral (~10^2 ppm Te and ~10^3 ppm Se). At the same time, the Woxi stibnite is characterized by high concentrations of As (~10^2 ppm) and elevated Hg (~10^1–10^2 ppm), but these elements are almost absent in the Olympiada minerals.

Cd, In, Sn, Hg, Mn also played an important role during the formation of mineral associations of the polymetallic sulfides and later sulfides stage, which are not typical for minerals of the early sulfides stage (Fig. 11). The distribution of these elements is mainly governed by crystal-chemical features. Thus, Cd and In are naturally enriched in sphalerite of both stages, while the other minerals concentrate them in smaller amounts. Sn has a different tendency, concentrating mainly in chalcopyrite, which agrees with data on its distribution in chalcopyrite with joint crystallization with sphalerite.

Elevated Cd and As concentrations are mainly observed in sphalerite formed by a low-temperature fluid, while Mn enrichment may indicate a relationship with magmatism (Belissont et al., 2014; Frenzel et al., 2016; Lee et al., 2019b; Zhuang et al., 2019; Xu et al., 2020a).

Mn significantly increases in berthierite, which is also due to crystal-chemical control. Berthierite with the content of up to 1.3 wt% Mn has been previously noted in the deposit. However, high concentrations of Mn may also be a feature of the fluids that formed the late mineral assemblage, where benavidesite ($Pb_4MnSb_6S_{14}$) and alabandite (MnS) were found in addition to Mn-berthierite, which may indicate a relationship with magmatism (Lee et al., 2019b).

Finally, the Hg content remains quite stable during the formation of mineralization of the polymetallic sulfides and late sulfides stage. This

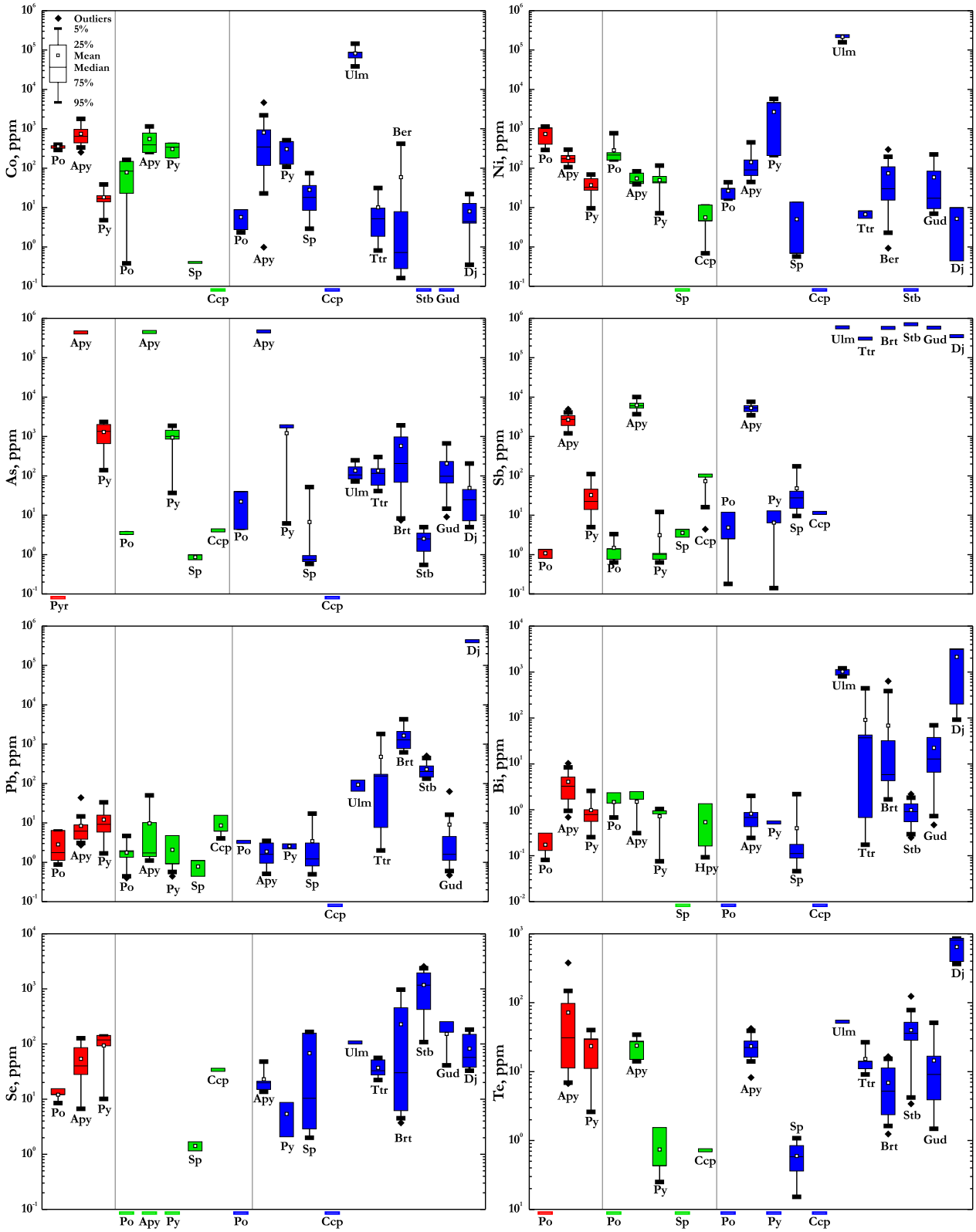

Fig. 10. Distribution of trace elements in minerals associations of different ages.

may be due to the involvement of the element in the ore process at later stages and its deposition not only in structurally bound form in sulfides, but also in its native form.

Probably, the listed elements played an insignificant role in the general balance of metals in ore fluids, since the most enriched minerals (sphalerite, chalcopyrite, tetrahedrite, jamesonite) are distributed in subordinate amounts. On the other hand, stibnite and berthierite are abundant in the association of late sulfides and are to some extent enriched in the listed elements. Despite the limited distribution of these elements, their distribution is extremely important in understanding the evolution of the fluid and the development of the ore system of the deposit.

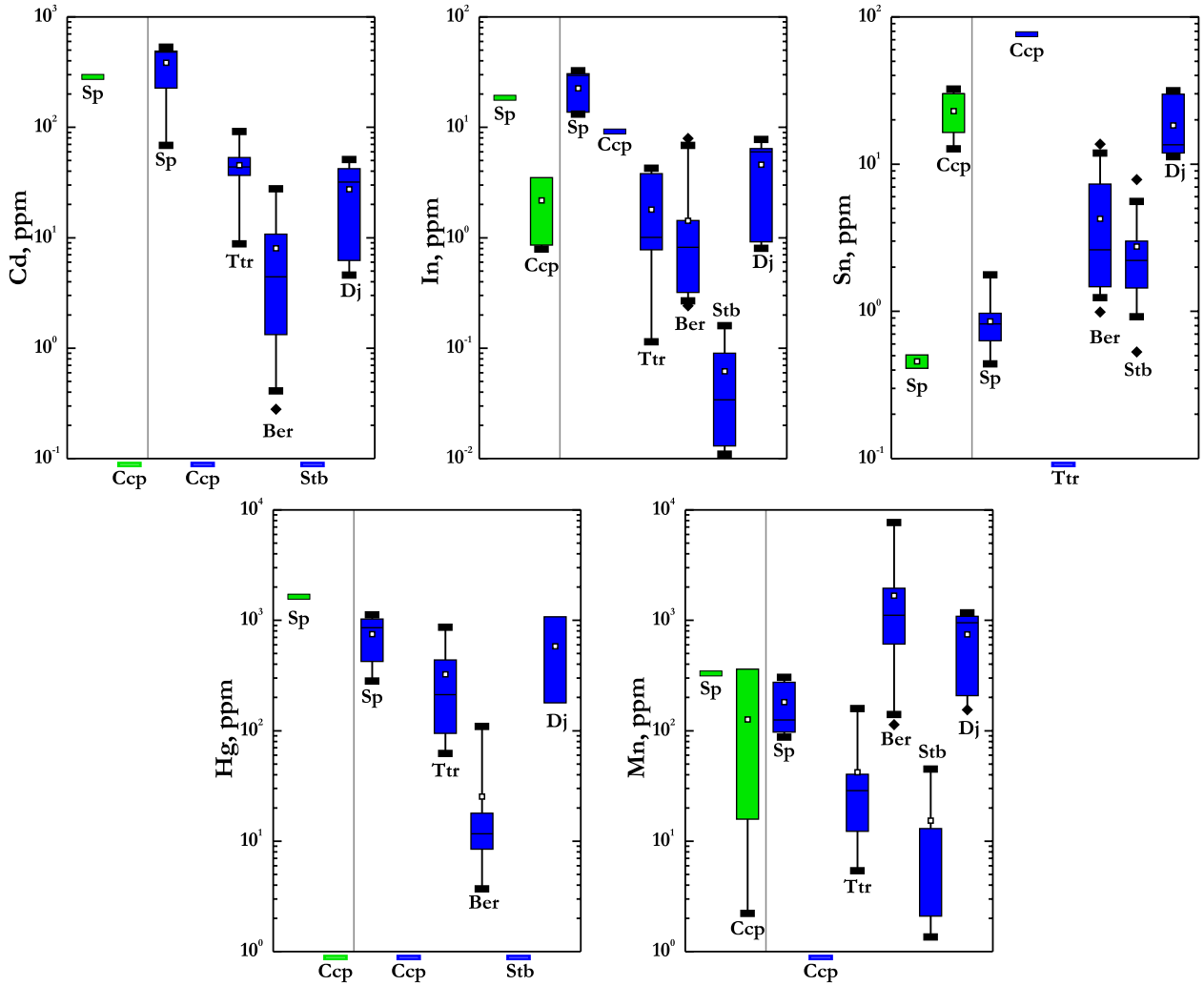

Fig. 11. Distribution of Cd, In, Sn, Hg, Mn in minerals of stages II and III.

Thus, the maximum amount of Au in acicular arsenopyrite occurs in a positive trend with the W content, as well as the increased Se and Te content in arsenopyrite I and pyrite I determine the ***As***-Au-W-Se-Te enrichment of the early sulfides stage, with arsenic occurring as a mineral-forming element and Au, W, Se and Te occurring as impurities. The presence of polymetallic sulfides and their microelement composition (increased concentrations of Hg, Cd, and In) allow us to allocate the ***Cu-Zn-Pb***-Cd-In enrichment of the polymetallic sulfides stage, where Cu, Zn, and Pb form their own minerals, and Cd and In are common as impurities. The features of the late sulfide stage are the maximum concentrations of Ag, Pb, Bi, and Te and elevated Hg concentrations. This, together with mineralogical features, determines the ***Sb-Co-Ni-Te-Bi-Pb-Hg***-Ag enrichment of this stage, while the presence of individual mineral phases has only not been determined for Ag.

6. Conclusions

Since the beginning of the study of the Olympiada deposit, three main models of the formation of the field have been proposed: (1) metamorphogenic-hydrothermal, based on the primary enrichment of metasedimentary strata with Au, its redistribution and concentration due to the processes of local metamorphism (Petrov, 1974; Grigorov, 2002); (2) magmatogenic-hydrothermal, linking the formation of the deposit with granitoid magmatism (Novozhilov & Gavrilov, 1999; Li, 2003; Korobeinikov et al., 2013); (3) polygenetic, including metamorphic, combining the previous two (Sazonov et al., 2010; Serdyuk et al., 2010; Sazonov et al., 2020). The metamorphogenic-hydrothermal model was further developed in works of R. Large and co-authors at the Sukhoi Log deposit (Large et al., 2011; Large et al., 2007). This model is now known as "*sedimentary metamorphic hydrothermal model (SMH)*".

Our data on the association of Au with W, Se, Te, Bi, Pb may indicate a relationship between mineralization and magmatism, but at the same time, these elements could be also be obtained from the host rocks. Early data also indicate the enrichment of the metasedimentary strata of the Kordinskaya Formation in Au up to 249 ppb (Sazonov et al., 2020).

On the other hand, despite more than half a century of study history, no synsedimentation framboidal pyrites enriched with gold have been found either in the ores or in the host rocks of the Olympiad (there are only single finds of metamorphosed pyrite nodules with quartz margins (Zvyagina, 1989). Gregory et al. (2019b) shows that the early pyrite can to be overgrown to form pyrite nodules, but to date there is no evidence of this process at the Olympiada). Such a find would serve as a strong argument in favor of the SMH model.

In favor of the connection of the deposit with magmatism, it is also indicated: finds in fluid inclusions of the deposit of halogenated hydrocarbons (Gibsher et al., 2019b); the proximity of the formation of mineralization in time to the formation of intrusions of granites of the Tatar-Ayakhta complex (Savichev, 2004); the presence within the ore field of deposits paragenetically associated with granitoids (Vysokoe-2 endocontact of granites; Olenye and Innokentievskoe – close exocontact) (Savichev et al., 2006).

Thus, today there is no clear and convincing evidence, as well as a

consensus on the genesis of the deposit, and each model has its supporters and opponents.

Based on the data obtained, as well as long-term geological observations, we suggest the following concept for the formation of the main concentrations of gold at the deposit.

The development of gold mineralization began with the deposition of acicular arsenopyrite I containing "invisible" gold. This arsenopyrite is characterized by sulfuric composition (S/As ~ 1.12; (S + As)/Fe ~ 2.04) and a low number of Fe atoms in the stoichiometric environment {3S3As} up to 65 % (Sazonov et al., 2020). The source of Au could be the meta-sedimentary rocks of the Korda suite, but the presence of positive trend between Au and granitophile W, as well as the features of the REE distribution in acicular arsenopyrite (Silyanov et al., 2021a) do not exclude the possibility of bringing some of Au from another, probably magmatic source.

Further development of the ore system led to hydrothermal metamorphism of early associations, which was accompanied by recrystallization of acicular arsenopyrite, release of Au and its re-deposition in a metal form (Fougerouse et al., 2016a; b). At the same time, arsenopyrite II and III sequentially approached the chemical (Apy-II S/As ~ 1.06; (S + As)/Fe ~ 2.03; Apy-III S/As ~ 0.98; (S + As)/Fe ~ 2.04) and structural (increase of the Fe share in position {3S3As} to ~ 74%) stoichiometry.

Remobilization and re-deposition of Au could be promoted by Bi, Pb, and Te, which, on the one hand, were also released during recrystallization of early sulfides, and, on the other hand, could be introduced into the system by new fluid influxes (Wagner et al., 2007; Fougerouse et al., 2016a; Wu et al., 2019; Gourcerol et al., 2020). The interaction of these elements with Au could lead to the formation of melt droplets directly in the hydrothermal solution and accumulation of all new gold portions by them — *hydrothermally-assisted melt-collector model* (Tooth et al., 2013; Belousov et al., 2016; Vikent'eva et al., 2018; Cave et al., 2019). As a result, Au-Bi-Pb alloys could be formed, the presence of which is shown in tetrahedrite (see Fig. 6). This mechanism may also be associated with the deposition of sporadic Bi-Te mineralization of the deposit.

In conclusion, evolution of ore process led to the enrichment of late stages with visible gold, as opposed to early stages, where "invisible" gold prevailed.

Declaration of Competing Interest

The authors declare that they have no known competing financial interests or personal relationships that could have appeared to influence the work reported in this paper.

Acknowledgements

We are grateful to reviewers and the Editorial Board members of the *OGR*, for their comments and improvements.

Funding

The reported study was funded by Russian Foundation for Basic Research (RFBR), project number 19-35-90017.

Appendix A. Supplementary data

Supplementary data to this article can be found online at https://doi.org/10.1016/j.oregeorev.2022.104750.

References

Arehart, G.B., Chryssoulis, S.L., Kesler, S.E., 1993. Gold and arsenic in iron sulfides from sediment hosted disseminated gold deposits: implication for depositional processes. Econ. Geol. Bull. Soc. Econ. Geol. 88, 171–185. https://doi.org/10.2113/gsecongeo.88.1.171.

Augustin, J., Gaboury, D., 2019. Multi-stage and multi-sourced fluid and gold in the formation of orogenic gold deposits in the world-class Mana district of Burkina Faso – Revealed by LA-ICP-MS analysis of pyrites and arsenopyrites. Ore Geol. Rev. 104, 495–521. https://doi.org/10.1016/j.oregeorev.2018.11.011.

Baranova, N.N., Afanas'eva, Z.B., Ivanova, G.F., Mironova, O.F., Kolpakova, N.N., 1997. Mineralization at the Olimpiada Au–(Sb–W) deposit: evidence from mineral parageneses and fluid inclusions. Geochem. Int. 35 (3), 239–249.

Belissont, R., Boiron, M.-C., Luais, B., Cathelineau, M., 2014. LA-ICP-MS analyses of minor and trace elements and bulk Ge isotopes in zoned Ge-rich sphalerites from the Noailhac – Saint-Salvy deposit (France): Insights into incorporation mechanisms and ore deposition processes. Geochim. Cosmochim. Acta. 126, 518–540. https://doi.org/10.1016/j.gca.2013.10.052.

Belousov, I., Large, R.R., Meffre, S., Danyushevsky, L.V., Steadman, J., Beardsmore, T., 2016. Pyrite compositions from VHMS and orogenic Au deposits in the Yilgarn Craton, Western Australia: Implications for gold and copper exploration. Ore Geol. Rev. 79, 474–499. https://doi.org/10.1016/j.oregeorev.2016.04.020.

Benzaazoua, M., Marion, P., Robaut, F., Pinto, A., 2007. Gold-bearing arsenopyrite and pyrite in refractory ores: analytical refinements and new understanding of gold mineralogy. Mineral. Mag. 71, 123–142. https://doi.org/10.1180/minmag.2007.071.2.123.

Bernatonis, P.B., 1999. Oxidation zone at the Olympiada disseminated gold-sulfide deposit: abstract of Candidate of Science Dissertation, Tomsk. Tomsk Polytechnic University 19, p in Russian.

Boiron, M.C., Cathelineau, M., Trescases, J.J., 1989. Conditions of gold-Bearing arsenopyrite crystallization in the Villeranges Basin, Marche-Combrailles shear zone, France: a mineralogical and fluid inclusion study. Econ. Geol. Bull. Soc. Econ. Geol. 84, 1340–1362. https://doi.org/10.2113/gsecongeo.84.5.1340.

Borisenko, A.S., Sazonov, A.M., Nevolko, P.A., Naumov, E.A., Tessalina, S., Kovalev, K. R., Sukhorukov, V.P., 2014. Gold deposits of the Yenisei Ridge (Russia) and age of its formation. Acta Geol. Sin. 88 (2), 686–687. https://doi.org/10.1111/1755-6724.12375_4.

Cabri, L.J., Newville, M., Gordon, R.A., Crozier, E., Sutton, S., Mcmahon, G., Jiang, D., 2000. Chemical speciation of gold in arsenopyrite. Can. Mineral. 38, 1265–1281. https://doi.org/10.2113/gscanmin.38.5.1265.

Cave, B.J., Barnes, S.-J., Pitcairn, I.K., Sack, P.J., Kuikka, H., Johnson, S.C., Duran, C.J., 2019. Multi-stage precipitation and redistribution of gold, and its collection by lead-bismuth and lead immiscible liquids in a reduced-intrusion related gold system (RIRGS); Dublin Gulch, western Canada. Ore Geol. Rev. 106, 28–55. https://doi.org/10.1016/j.oregeorev.2019.01.010.

Chouinard, A., Paquette, A., Williams-Jones, A.E., 2005. Crystallographic controls on trace-element incorporation in Auriferous pyrite from the Pascua epithermal high-sulfidation deposit, Chile-Argentina. Can. Mineral. 43, 951–963. https://doi.org/10.2113/gscanmin.43.3.951.

Conn, C.D., Spry, P.G., Layton-Matthews, D., Voinot, A., Koenig, A., 2019. The effects of amphibolite facies metamorphism on the trace element composition of pyrite and pyrrhotite in the Cambrian Nairne Pyrite Member, Kanmantoo Group, South Australia. Ore Geol. Rev. 114, 103–128. https://doi.org/10.1016/j.oregeorev.2019.103128.

Cook, N.J., Chryssoulis, N.J., 1990. Concentrations of "Invisible Gold" in the common sulfides. Can. Miner. 28, 1–16.

Cook, N.J., Ciobanu, C.L., Pring, A., Skinner, W., Shimizu, M., Danyushevsky, L., Saini-Eidukat, B., Melcher, F., 2009. Trace and minor elements in sphalerite: a LA-ICPMS study. Geochim. Cosmochim. Acta. 73, 4761–4791. https://doi.org/10.1016/j.gca.2009.05.045.

Deditius, A.P., Utsunomiya, S., Renock, D., Ewing, R.C., Ramana, C.V., Becker, U., Kesler, S.E., 2008. A proposed new type of arsenian pyrite: Composition, nanostructure and geological significance. Geochim. Cosmochim. Acta. 72, 2919–2933. https://doi.org/10.1016/j.gca.2008.03.014.

Dehnavi, A.S., McFarlane, C.R.M., Lentz, D.R., Walker, J.A., 2018. Assessment of pyrite composition by LA-ICP-MS techniques from massive sulfide deposits of the Bathurst Mining Camp, Canada: from textural and chemical evolution to its application as a vectoring tool for the exploration of VMS deposits. Ore Geol. Rev. 92, 656–671. https://doi.org/10.1016/j.oregeorev.2017.10.010.

Ebel, D.S., Sack, R.O., 1991. Arsenic-Ag incompatibility in fahlore. Mineral. Mag. 55, 521–528. https://doi.org/10.1180/minmag.1991.055.381.04.

Fleet, M.E., Mumin, H., 1997. Gold-bearing arsenian pyrite and marcasite and arsenopyrite from Carlin Trend gold deposits and laboratory synthesis. Am. Mineral. 82, 182–193.

Fougerouse, D., Micklethwaite, S., Tomkins, A.G., Mei, Y., Kilburn, M., Guagliardo, P., Fisher, L.A., Halfpenny, A., Gee, M., Paterson, D., Howard, D.L., 2016a. Gold remobilisation and formation of high grade ore shoots driven by dissolution-reprecipitation replacement and Ni substitution into auriferous arsenopyrite. Geochim. Cosmochim. Acta 178, 143–159. https://doi.org/10.1016/j.gca.2016.01.040.

Fougerouse, D., Reddy, S.M., Saxey, D.W., Saxey, D.W., Rickard, W.D.A., van Riessen, A., Micklethwaite, S., 2016b. Nanoscale gold clusters in arsenopyrite controlled by growth rate not concentration: evidence from atom probe microscopy. Am. Mineral. 101, 1916–1919. https://doi.org/10.2138/am-2016-5781CCBYNCND.

Frenzel, M., Hirsch, T., Gutzmer, J., 2016. Gallium, germanium, indium, and other trace and minor elements in sphalerite as a function of deposit type – A meta-analysis. Ore Geol. Rev. 76, 52–78. https://doi.org/10.1016/j.oregeorev.2015.12.017.

Fu, S., Hu, R., Bi, X., Sullivan, N.A., Yan, J., 2020. Trace element composition of stibnite: substitution mechanism and implications for the genesis of Sb deposits in southern China. Appl. Geochem. 118, 104637 https://doi.org/10.1016/j.apgeochem.2020.104637.

Genkin, A.D., Bortnikov, N.S., Cabri, L.J., Wagner, F.E., Stanley, C.J., Safonov, Y.G., McMahon, G., Friedl, J., Kerzin, A.L., Gamyanin, G.N., 1998. A multidisciplinary study of invisible gold in arsenopyrite from four mesothermal gold deposits in Siberia. Russian Federation. Econ. Geol. 93 (4), 463–487. https://doi.org/10.2113/gsecongeo.93.4.463.

Genkin, A.D., Lopatin, V.A., Savel'ev, R.A., Safonov, Y.G., Sergeev, N.B., Kerzin, A.L., Tsepin, A.I., Amshtutz, Kh., Afanas'eva, Z.B., Wagner, F.E., Ivanova, G.F., 1994. Gold ores of the Olimpiada deposit (Enisei range, Siberia). Geol. Ore Dep. 36 (2), 101–123.

Genkin, A.D., Wagner, F., Krylova, T.L., Tsepin, A.I., 2002. Auriferous arsenopyrite and conditions of its formation at the Olympiada and Veduga gold deposits (Yenisei Ridge, Siberia). Geologia Rudnykh Mestorozhdeniy. 44, 59–76 in Russian.

George, L.L., Cook, N.J., Crowe, B.B.P., Ciobanu, C.L., 2018. Trace elements in hydrothermal chalcopyrite. Mineral. Mag. 82 (1), 59–88. https://doi.org/10.1180/minmag.2017.081.021.

Gibsher, N.A., Sazonov, A.M., Travin, A.V., Tomilenko, A.A., Ponomarchuk, A.V., Sil'yanov, S.A., Nekrasova, N.A., Shaparenko, E.O., Ryabukha, M.A., Khomenko, M. O., 2019a. Age and duration of the formation of the Olimpiadinski gold deposit (Yenisei ridge, Russia). Geochem. Int. 57, 593–599. https://doi.org/10.31857/S0016-7525645548-553.

Gibsher, N.A., Tomilenko, A.A., Sazonov, A.V., Bul'bak, T.A., Ryabukha, M.A., Sil'yanov, S.A., Nekrasova, N.A., Khomenko, M.O., Shaparenko, E.O., 2019b. The Olimpiada gold deposit (Yenisei ridge): temperature, pressure, composition of ore-forming fluids, $\delta^{34}S$ in sulfides, $^{3}He/^{4}He$ of fluids, Ar-Ar age and duration of deposit formation. Russ. Geol. Geophys. 9, 1310–1330. https://doi.org/10.15372/GiG2019073.

Goldfarb, R.J., Groves, D.I., 2015. Orogenic gold: Common or evolving fluid and metal sources through time. Lithos. 233, 2–26. https://doi.org/10.1016/j.lithos.2015.07.011.

Goldfarb, R.J., Baker, T., Dubé B., Groves, M.D., Hart-Katuin, C., Gosselin P., 2005. Distribution, Character, and Genesis of Gold Deposits in Metamorphic Terranes, in Hedenquist, J.W., Thompson, J.F.H., Goldfarb, R.J., Richards, J.P. (Eds.), Economic Geology One Hundredth Anniversary Volume. Society of Economic Geologists. pp. 407–450.

Gourcerol, B., Kontak, D.J., Petrus, J.A., 2020. Thurston application of LA ICP-MS analysis of arsenopyrite to gold metallogeny of the Meguma Terrane, Nova Scotia, Canada. Gondwana Res. 81, 265–290. https://doi.org/10.1016/j.gr.2019.11.011.

Gregory, D.D., Cracknell, M.J., Large, R.R., McGoldrick, P., Kuhn, S.D., Maslennikov, V. V., Baker, M.J., Fox, N., Belousov, I., Figueroa, M.C., Steadman, J.A., Fabris, A.J., Lyons, T.W., 2019a. Distinguishing ore deposit type and barren sedimentary pyrite using laser ablation-inductively coupled plasma-mass spectrometry trace element data and statistical analysis of large data sets. Econ. Geol. 114, 771–786. https://doi.org/10.5382/econgeo.4654.

Gregory, D.D., Large, R.R., Bath, A.B., Steadman, J.A., Wu, S., Danyushevsky, L., Bull, S. W., Holden, P., Ireland, T.R., 2016. Trace Element Content of Pyrite from the Kapai Slate, St. Ives Gold District, Western Australia. Econ. Geol. 111, 1297–1320. https://doi.org/10.2113/econgeo.111.6.1297.

Gregory, D.D., Large, R.R., Halpin, J.A., Baturina, E.L., Lyons, T.W., Wu, S., Danyushevsky, L., Sack, P.J., Chappaz, A., Maslennikov, V.V., Bull, S.W., 2015. Trace element content of sedimentary pyrite in black shales. Econ. Geol. 110, 1389–1410. https://doi.org/10.2113/econgeo.110.6.1389.

Gregory, D.D., Mukherjee, I., Olson, S.L., Large, R.R., Danyushevsky, L.V., Stepanov, A. S., Avila, J.N., Cliff, J., Ireland, T.R., Raiswell, R., Olin, P.H., Maslennikov, V.V., Lyons, T.W., 2019b. The formation mechanisms of sedimentary pyrite nodules determined by trace element and sulfur isotope microanalysis. Geochim. Cosmochim. Acta. 259, 53–68. https://doi.org/10.1016/j.gca.2019.05.035.

Grigorov, V.T., 2002. The biggest gold-ore deposits of the Yenisei Mountain Range and Kuznetsky Alatau and their economic estimation from a position of stratiform ore-forming. Scientific World, Moscow, p. 168 p. in Russian.

Hart, C.J.R., 2005. Reduced intrusion-related gold systems, in Goodfellow, W.D. (Ed.), Mineral deposits of Canada; A synthesis of major deposit-types, district metallogeny, the evolution of geological provinces, and exploration methods: Geological Association of Canada, Mineral Deposits Division, Special Publication No. 5.pp. 95–112.

Keith, M., Smith, D.J., Jenkin, G.R.T., Holwell, D.A., Dye, M.D., 2018. A review of Te and Se systematics in hydrothermal pyrite from precious metal deposits: Insights into ore-forming processes. Ore Geol. Rev. 96, 269–282. https://doi.org/10.1016/j.oregeorev.2017.07.023.

Kirik, S.D., Sazonov, A.M., Silyanov, S.A., Bayukov, O.A., 2017. Investigation of disordering in natural arsenopyrite by X-ray powder crystal structure analysis and nuclear gamma resonance. J. Sib. Fed. Univ. Eng. Technol. Ser. 10, 578–592. (In Russian) 10.17516/1999-494X-2017-10-5-578-592.

Konstantinov, M.M., Cherkasov, S.V., Dankovtsov, R.F., Egorkin, A.V., 1999. Specific crustal features for large and superlarge endogenic gold deposits (Siberia and Far East regions). Global Tectonics and Metallogeny. 7, 143–147 in Russian.

Korobeinikov, A.F., Ananiev, Y.S., Gusev, A.I., Voroshilov, V.G., Nomokonova, G.G., Pshenichkin, A.Y., and Timkin, T.V., 2013. Ore-metasomatic system and geochemical zonation of goldfields and deposits in the fold belts of Siberia. Tomsk, Tomsk Polytechnic University, 458 p. (in Russian).

Kozlov, P.S., Filippov, Y.F., Likhanov, I.I., Nozhkin, A.D., 2020. Geodynamic model of the neoproterozoic evolution of the Yenisei Paleosubduction Zone (Western Margin of the Siberian Craton), Russia. Geotecton. 54, 54–67. https://doi.org/10.1134/S0016852120010069.

Kravtsova, R.G., Tauson, V.L., Nikitenko, E.M., 2015. Modes of Au, Pt, and Pd occurrence in arsenopyrite from the Natalkinskoe deposit, NE Russia. Geochem. Int. 53 (11), 964–972. https://doi.org/10.1134/S0016702915090037.

Kravtsova, R.G., Tauson, V.L., Goryachev, N.A., Makshakov, A.S., Lipko, S.V., Arsent'ev, K.Y., 2020. SEM study of the surface of arsenopyrite and pyrite from the natalkinskoe deposit, Northeastern Russia. Geochem. Int. 58, 531–538. https://doi.org/10.1134/S0016702920050031.

Kuzmichev, A.B., Sklyarov, E.V., 2016. The Precambrian of Transangaria, Yenisei Ridge (Siberia): Neoproterozoic microcontinent, Grenville-age orogen, or reworked margin of the Siberian craton? J. Asian Earth Sci. 115, 419–441. https://doi.org/10.1016/j.jseaes.2015.10.017.

Large, R.R., Bull, S.W., Maslennikov, V.V., 2011. A carbonaceous sedimentary source-rock model for carlin-type and orogenic gold deposits. Econ. Geol. 106, 331–358. https://doi.org/10.2113/econgeo.106.3.331.

Large, R.R., Maslennikov, V.V., 2020. Invisible gold paragenesis and geochemistry in pyrite from orogenic and sediment-hosted gold deposits. Minerals 10, 339. https://doi.org/10.3390/min10040339.

Large, R.R., Maslennikov, V.V., Robert, F., Danyushevsky, L.D., Chang, Z., 2007. Multistage sedimentary and metamorphic origin of pyrite and gold in the giant sukhoi log deposit, Lena Gold Province, Russia. Econ. Geol. 102, 1233–1267. https://doi.org/10.2113/gsecongeo.102.7.1233.

Lee, M., Shin, D., Yoo, B., Im, H., Pak, S., Choi, S., 2019a. LA-ICP-MS trace element analysis of arsenopyrite from the Samgwang gold deposit, South Korea, and its genetic implications. Ore Geol. Rev. 114, 103147 https://doi.org/10.1016/j.oregeorev.2019.103147.

Lee, M., Yoo, B.C., Yang, Y.-S., Lee, T.H., Seo, J.H., 2019b. Sphalerite geochemistry of the Zn-Pb orebodies in the Taebaeksan metallogenic province. Korea. Ore Geol. Rev. 107, 1046–1067. https://doi.org/10.1016/j.oregeorev.2019.03.030.

Li, L.V., 2003. The Olympiada disseminated gold-sulfide deposit: Krasnoyarsk, KNIIGiMS, 120 p. (in Russian).

Likhanov, I.I., Nozhkin, A.D., Reverdatto, V.V., Kozlov, P.S., 2014. Grenville tectonic events and evolution of the yenisei ridge at the Western Margin of the Siberian Craton. Geotectonics 48 (5), 371–389. https://doi.org/10.1134/S0016852114050045.

Longerich, H.P., Jackson, S.E., Günther, D., 1996. Inter-laboratory note. Laser ablation inductively coupled plasma mass spectrometric transient signal data acquisition and analyte concentration calculation. J. Anal. Atomic Spectrom. 11, 899–904. https://doi.org/10.1039/ja9961100899.

Maslennikov, V.V., Maslennikova, S.P., Large, R.R., Danyushevsky, L.V., Herrington, R. J., Ayupova, N.R., Zaykov, V.V., Lein, A.Y., Tseluyko, A.S., Melekestseva, I.Y., Tessalina, S.G., 2017. Chimneys in Paleozoic massive sulfide mounds of the Urals VMS deposits: mineral and trace element comparison with modern black, grey, white and clear smokers. Ore Geol. Rev. 85, 64–106. https://doi.org/10.1016/j.oregeorev.2016.09.012.

McClenaghan, S.H., Lentz, D.R., Cabri, L.J., 2004. Abundance and speciation of gold in massive sulfides of the Bathurst Mining Camp, New Brunswick, Canada. Can. Mineral. 42, 851–871. https://doi.org/10.2113/gscanmin.42.3.851.

McFarlane, C.R., Mavrogenes, J., Lentz, D., King, K., Allibone, A., Holcombe, R., 2011. Geology and intrusion-related affinity of the Morila gold mine, southeast Mali. Econ. Geol. 106, 727–750. https://doi.org/10.2113/econgeo.106.5.727.

Meffre, S., Large, R.R., Steadman, J.A., Gregory, D.D., Stepanov, A.S., Kamenetsky, V.S., Ehrig, K., Scott, R.J., 2016. Multi-stage enrichment processes for large gold-bearing ore deposits. Ore Geol. Rev. 76, 268–279. https://doi.org/10.1016/j.oregeorev.2015.09.002.

Merkulova, M., Mathon, O., Glatzel, P., Rovezzi, M., Batanova, V., Marion, P., Boiron, M.-C., Manceau, A., 2019. Revealing the chemical form of "invisible" gold in natural arsenian pyrite and arsenopyrite with high energy-resolution X-ray absorption spectroscopy. ACS Earth Space Chem. 3 (9), 1905–1914. https://doi.org/10.1021/acsearthspacechem.9b00099.

Metelkin, D.V., Vernikovsky, V.A., Kazansky, A.Y., 2007. Neoproterozoic evolution of Rodinia: constraints from new paleomagnetic data on the western margin of the Siberian. Russ. Geol. Geophys. 48, 32–45. https://doi.org/10.1016/j.rgg.2006.12.004.

Morey, A.A., Tomkins, A.G., Bierlein, F.G., Weinberg, R.F., Davidson, G.J., 2008. Bimodal distribution of gold in pyrite and arsenopyrite: examples from the Archean Boorara and Bardoc shear zones, Yilgarn craton, Western Australia. Econ. Geol. 103, 599–614. https://doi.org/10.2113/gsecongeo.103.3.599.

Mumin, A.H., Fleet, M.E., Chryssoulis, S.L., 1994. Gold mineralization in As-rich mesothermal gold ores of the Bogosu-Prestea mining district of the Ashanti Gold Belt, Ghana: remobilization of "invisible" gold. Miner. Depos. 29, 445–460. https://doi.org/10.1007/BF00193506.

Murakami, H., Ishihara, S., 2013. Trace elements of Indium-bearing sphalerite from tin-polymetallic deposits in Bolivia, China and Japan: a femto-second LA-ICPMS study. Ore Geol. Rev. 53, 223–243. https://doi.org/10.1016/j.oregeorev.2013.01.010.

Naumov, E.A., Borisenko, A.S., Nevolko, P.A., Kovalev, K., Tessalina, S., Sazonov, A., Savichev, A., 2015. Gold-sulfide (Au-As) Deposits of the Yenisei Ridge (Russia): Age, Sources of Metals and Nature of Fluids. In: Proceedings of the 13th SGA Biennial Meeting, pp. 165–168.

Nekrasov, I.Ya., 1991. Geochemistry, mineralogy and genesis of gold deposits: Moscow, Science, 302 p. (in Russian).

Novozhilov, Y.I., and Gavrilov, A.M., 1999. Gold-sulfide deposits in carbonaceous-clastic formations: Moscow, TsNIGRI, 175 p. (in Russian).

Novozhilov, Y.I., Gavrilov, A.M., Yablokova, S.V., 2014. V.I.The unique au-sulfide deposit Olympiada in neoproterozoic terrigenous sequence. Rudy i Metally. 3, 51–64 in Russian.

Nozhkin, A.D., Borisenko, A.S., Nevolko, P.A., 2011. Stages of the Late Proterozoic magmatism and ages of gold mineralization in the Yenisei Ridge. Russ. Geol. Geophys. 52, 158–181. https://doi.org/10.1016/j.rgg.2010.12.010.

Nozhkin, A.D., Likhanov, I.I., Bayanova, T.B., Serov, P.A., 2017. First data on late vendian granitoid magmatism of the northwestern Sayan-Yenisei accretionary belt. Geochem. Int. 55, 792–801. https://doi.org/10.1134/S0016702917070072.

Paktunc, D., Kingston, D., Pratt, A., McMullen, J., 2006. Distribution of gold in pyrite and in products of its transformation resulting from roasting of refractory gold ore. Can. Mineral. 44, 213–227. https://doi.org/10.2113/gscanmin.44.1.213.

Palenik, C.S., Utsunomiya, S., Reich, M., Kesler, S.E., Wang, L., Ewing, R.C., 2004. «Invisible» gold revealed: direct imaging of gold nanoparticles in a Carlin-type deposit. Am. Mineral. 89, 1359–1366. https://doi.org/10.2138/am-2004-1002.

Pals, D.W., Spry, P.G., Chryssouls, S., 2003. Invisible gold and tellurium in arsenic-rich pyrite from the Emperor gold deposit, Fiji: implications for gold distribution and deposition. Econ. Geol. Bull. Soc. Econ. Geol. 98, 479–493. https://doi.org/10.2113/gsecongeo.98.3.479.

Paton, C., Hellstrom, J., Paul, B., Woodhead, J., Hergt, J., 2011. Iolite: freeware for the visualisation and processing of mass spectrometric data. J. Anal. Atomic Spectrom. 26, 2508–2518. https://doi.org/10.1039/C1JA10172B.

Petrov, V.G., 1974. Gold metallogeny of the northern Yenisei Ridge: Novosibirsk, Nauka, 140 p. (in Russian).

Pitcairn, I.K., Teagle, D.A.H., Craw, D., Olivo, G.R., Kerrich, R., Brewer, T.S., 2006. Sources of metals and fluids in orogenic gold deposits: insights from the Otago and Alpine Schists, New Zealand. Econ. Geol. 101, 1525–1546. https://doi.org/10.2113/gsecongeo.101.8.1525.

Pokrovski, G.S., Kokh, M.A., Proux, O., Hazemann, J.-L., Bazarkina, E.F., Testemale, D., Escoda, C., Boiron, M.-C., Blanchard, M., Aigouy, T., Gouy, S., de Parseval, P., Thibaut, M., 2019. The nature and partitioning of invisible gold in the pyrite-fluid system. Ore Geol. Rev. 109, 545–563. https://doi.org/10.1016/j.oregeorev.2019.04.024.

Reich, M., Kesler, S.E., Utsunomiya, S., Palenik, C.S., Chryssoulis, S.L., Ewing, R.C., 2005. Solubility of gold in arsenian pyrite. Geochim. Cosmochim. Acta 69, 2781–2796. https://doi.org/10.1016/j.gca.2005.01.011.

Savichev, A.A., 2004. Mineralogical-geochemical zoning and conditions for the formation of Au-Sb-W mineralization of the Verkhne-Yenashim ore cluster (Yenisei ridge). PhD thesis: St. Petersburg. 24 p. (in Russian).

Savichev, A.A., Gavrilenko, V.V., 2003. Gold-sulfide mineralization of the North-Yenisei region (Siberia) and the conditions of its formation. Proceedings of the Russian Mineralogical Society. 2, 15–32. (in Russian).

Savichev, A.A., Shevchenko, S.S., Rozinov, M.I., 2006. Isotopic and petrogeochemical characteristics of the Olympiada gold-sulfide deposit and its satellites (Yenisei Range). Regional Geol. Metallogeny 28, 122–143 in Russian.

Sazonov, A.M., Ananyev, A.A., Poleva, T.V., Khokhlov, A.N., Vlasov, V.S., Zvyagina, E.A., Fedorova, A.V., Tishin, P.A., Leontyev, S.I., 2010. Gold-ore metallogeny of the Yenisey Ridge: geological-structural provincialism, structural types of ore fields. J. Sib. Fed. Univ. Eng. Technol. Ser. 4, 371–395 in Russian.

Sazonov, A.M., Kirik, S.D., Silyanov, S.A., Bayukov, O.A., Tushin, P.A., 2016. Typomorphism of arsenopyrite from Blagodatnoye and Olimpiada gold ore deposits (Yenisei Ridge). Mineralogy. 3, 52–70. In Russian.

Sazonov, A.M., Lobanov, K.V., Zvyagina, E.A., Leontiev, S.I., Silyanov, S.A., Nekrasova, N.A., Nekrasov, A.Y., Borodushkin, A.B., Poperekov, V.A., Zhuravlev, V.V., Ilyin, S. S., Kalinin, Yu.A., Savichev, A.A., Yakubchuk, A.S., 2020. Olympiada Gold Deposit, Yenisei Ridge, Russia, in Sillitoe, R.H., Goldfarb, R.J., Robert, F., Simmons, S.F. (Eds.), Geology of the world's major gold deposits and provinces, Soc. of Econ. Geologists Spec. Publ. 23, 203–226. 10.5382/SP.23.10.

Sazonov, A.M., Silyanov, S.A., Bayukov, O.A., Knyazev, Y.V., Zvyagina, Y.A., Tishin, P. A., 2019a. Composition and ligand microstructure of arsenopyrite from gold ore deposits of the Yenisei Ridge (Eastern Siberia, Russia). Minerals 9, 737. https://doi.org/10.3390/min9120737.

Sazonov, A.M., Zvyagina, Ye.A., Silyanov, S.A., Lobanov, K.V., Leontyev, S.I., Kalinin Yu. A., Savichev, A.A., Tishin, P.A., 2019b. Ore genesis of the Olimpiada gold deposit (Yenisei Ridge, Russia). Geosph. Res. 1, 17–43. (In Russian) 10.17223/25421379/9/2.

Serdyuk, S.S., Komorovskiy, Yu.E., Zverev, A.I., Oyaber', V.K., Vlasov, V.S., Babushkin, V.E., Kirilenko, V.A., and Zemlyanskiy, S.A., 2010. Models of gold deposits in the Yenisei area of Siberia: Krasnoyarsk, Institute Gornogo Dela, Geologii i Geotekhnologiy, 582 p. (in Russian).

Silyanov, S.A., Sazonov, A.M., Tishin, P.A., Lobastov, B.M., Nekrasova, N.A., Zvyagina, E. A., Ryabukha, M.A., 2021a. Trace elements in sulfides and gold of the olimpiada deposit (Yenisei Ridge): ore substance sources and fluid parameters. Russ. Geol. Geophys. 62 (3), 306–323. https://doi.org/10.2113/RGG20194105.

Silyanov, S.A., Sazonov, A.M., Zvyagina, Y.A., Savichev, A.A., Lobastov, B.M., 2021b. Gold in the oxidized ores of the olympiada deposit (Eastern Siberia, Russia). Minerals. 11 (2), 190. https://doi.org/10.3390/min11020190.

Sovmen, V.K., Stragis, Y.M., Plekhanov, A.A., Bibik, S.M., Krovyakova, L.P., Savushkina, S.I., Lokhmakov, V.A., Zvezdin, I.G., and Logachev, V.S., 2009. Geological structure of gold deposits and experience of geological work at Polyus Company in the Krasnoyarsk region: Krasnoyarsk, Verso, 208 p. (in Russian).

Simon, G., Huang, H., Penner-Hahn, J.E., Kesler, S.E., Kao, L.-I., 1999. Oxidation state of gold and arsenic in gold-bearing arsenian pyrite. Am. Mineral. 84, 1071–1079. https://doi.org/10.2138/am-1999-7-809.

Sung, Y.H., Brugger, J., Ciobanu, C.L., Pring, A., Skinner, W., Nugus, M., 2009. Invisible gold in arsenian pyrite and arsenopyrite from a multistage Archaean gold deposit: sunrise Dam, Eastern Goldfields Province, Western Australia. Miner. Deposita. 44, 765–791. https://doi.org/10.1007/s00126-009-0244-4.

Thomas, H.V., Large, R.R., Bullm, S.W., Maslennikov, V., Berry, R.F., Fraser, R., Froud, S., Moye, R., 2011. Pyrite and pyrrhotite textures and composition in sediments, laminated quartz veins, and reefs at bendigo gold mine, Australia: insights for ore genesis. Econ. Geol. 106 (1), 1–31. https://doi.org/10.2113/econgeo.106.1.1.

Tooth, B., Etschmann, B., Pokrovski, G.S., Testemale, D., Hazemann, J.-L., Grundler, P. V., Brugger, J., 2013. Bismuth speciation in hydrothermal fluids: an X-ray absorption spectroscopy and solubility study. Geochim. Cosmochim. Acta. 101, 156–172. https://doi.org/10.1016/j.gca.2012.10.020.

Trigub, A.L., Tagirov, B.R., Kvashnina, K.O., Chareev, D., Nickolsky, M., Shiryaev, A.A., Baranova, N., Kovalchuk, E., Mokhov, A., 2017. X-ray spectroscopy study of the chemical state of "invisible" Au in synthetic minerals in the Fe-As-S system. Am. Mineral. 102, 1057–1065. https://doi.org/10.2138/am-2017-5832.

Vernikovsky, V.A., Metelkin, D.V., Vernikovskaya, A.E., Matushkin, N.Y., Kazansky, A.Y., Kadilnikov, P.I., Romanova, I.V., Wingate, M.T.D., Larionov, A.N., Rodionov, N.V., 2016. Neoproterozoic tectonic structure of the Yenisei Ridge and formation of the western margin of the Siberian craton based on new geological, paleomagnetic, and geochronological data. Russ. Geol. Geophys. 57, 47–68. https://doi.org/10.1016/j.rgg.2016.01.004.

Vernikovsky, V.A., Vernikovskaya, A.E., Kotov, A.B., Salnikova, E.B., Kovach, V.P., 2003. Neoproterozoic accretionary and collisional events on the western margin of the Siberian craton: new geological and geochronological evidence from the Yenisey Ridge. Tectonophysics 375, 147–168. https://doi.org/10.1016/S0040-1951(03)00337-8.

Vernikovsky, V.A., Vernikovskaya, A.E., 2006. Tectonics and evolution of the granitoid magmatism in the Yenisei Ridge. Russ. Geol. Geophys. 47 (1), 35–52.

Vikent'eva, O.V., Prokofiev, V.Y., Gamyanin, G.N., Goryachev, N.A., Bortnikov, N.S., 2018. Intrusion-related gold-bismuth deposits of North-East Russia: PTX parameters and sources of hydrothermal fluids. Ore Geol. Rev. 102, 240–259. https://doi.org/10.1016/j.oregeorev.2018.09.004.

Voute, F., Hagemann, S.G., Evans, N.J., Villanes, C., 2019. Sulfur isotopes, trace element, and textural analyses of pyrite, arsenopyrite and base metal sulfides associated with gold mineralization in the Pataz-Parcoy district, Peru: implication for paragenesis, fluid source, and gold deposition mechanisms. Miner. Deposita 54, 1077–1100. https://doi.org/10.1007/s00126-018-0857-6.

Wagner, T., Klemd, R., Wenzel, T., Mattsson, B., 2007. Gold upgrading in metamorphosed massive sulfide ore deposits: Direct evidence from laser-ablation–inductively coupled plasma–mass spectrometry analysis of invisible gold. Geology 35 (9), 775–778. https://doi.org/10.1130/G23739A.1.

Wei, C., Ye, L., Hu, Y., Danyushevskiy, L., Li, Z., Huang, Z., 2019. Distribution and occurrence of Ge and related trace elements in sphalerite from the Lehong carbonate-hosted Zn-Pb deposit, northeastern Yunnan, China: insights from SEM and LA-ICP-MS studies. Ore Geol. Rev. 115, 103175 https://doi.org/10.1016/j.oregeorev.2019.103175.

Wilson, S.A., Ridley, W.I., Koenig, A.E., 2002. Development of sulphide calibration standards for the laser ablation inductively-coupled plasma mass spectrometry technique. J. Anal. At. Spectrom. 17, 406–409. https://doi.org/10.1039/B108787H.

Wu, Y.-F., Evans, K., Li, J.-Y., Fougerouse, D., Large, R.R., Guagliardo, P., 2019. Metal remobilization and ore-fluid perturbation during episodic replacement of auriferous pyrite from an epizonal orogenic gold deposit. Geochim. Cosmochim. Acta 245, 98–147. https://doi.org/10.1016/j.gca.2018.10.031.

Xu, J., Cook, N.J., Ciobanu, C.L., Li, X., Kontonikas-Charos, A., Gilbert, S., Lv, Y., 2020. Indium distribution in sphalerite from sulfide–oxide–silicate skarn assemblages: a case study of the Dulong Zn–Sn–In deposit, Southwest China. Miner. Deposita. 10.1007/s00126-020-00972-y.

Xu, N., Wu, C.-L., Li, S.-R., Xue, B.-Q., He, X., Yu, Y.-L., Liu, J.-Z., 2020b. LA-ICP-MS in situ analyses of the pyrites in Dongyang gold deposit, Southeast China: implications to the gold mineralization. China Geol. 1, 1–17. https://doi.org/10.31035/cg2018123.

Yakubchuk, A., Stein, H., Wilde, A., 2014. Results of pilot Re-Os dating of sulfides from the Sukhoi Log and Olympiada orogenic gold deposits, Russia. Ore Geol. Rev. 59, 21–28. https://doi.org/10.1016/j.oregeorev.2013.12.003.

Zabiyaka, A.I., Kurgankov, P.P., Gusarov, Yu.V., et al., 2004, Tectonics and metallogeny of the Lower Angara region: Krasnoyarsk, KNIIGiMS, 322 p. (in Russian).

Zhang, Y., Chu, F., Li, Z., Dong, Y., Wang, H., Li, X., Long, J., 2020. Gold enrichment in hydrothermal sulfides from the Okinawa Trough: an in situ LA-ICP-MS study. Ore Geol. Rev. 116, 103255 https://doi.org/10.1016/j.oregeorev.2019.103255.

Zhuang, L., Song, Y., Liu, Y., Fard, M., Hou, Z., 2019. Major and trace elements and sulfur isotopes in two stages of sphalerite from the world-class Angouran Zn–Pb deposit, Iran: implications for mineralization conditions and type. Ore Geol. Rev. 109, 184–200. https://doi.org/10.1016/j.oregeorev.2019.04.009.

Zvyagina, E.A., 1989. Metamorphism and gold metallogeny of the Upper Enashimo ore cluster: Candidate of Science Dissertation, Krasnoyarsk, Siberian Federal University, 275 p. (In Russian).